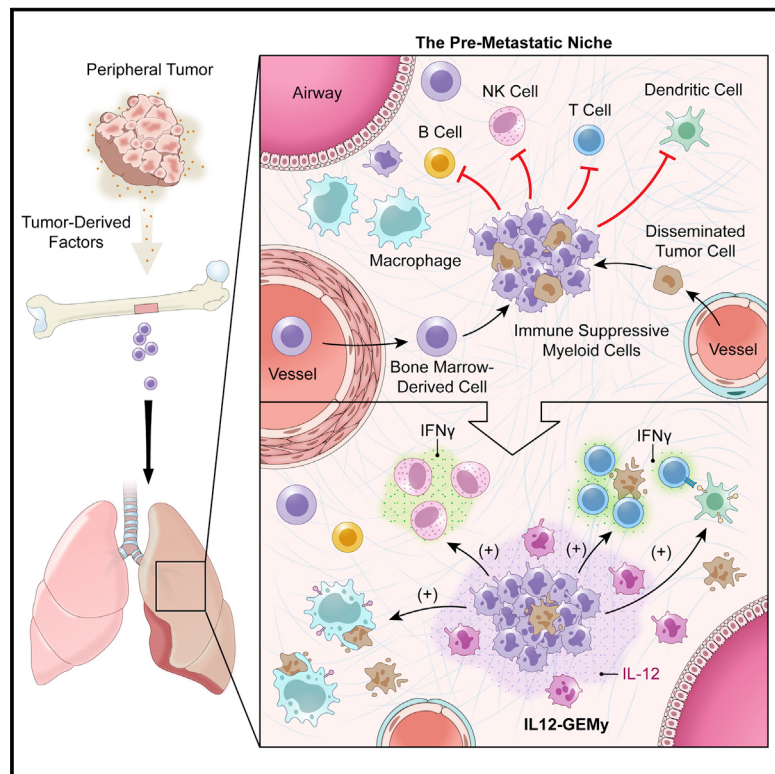


Genetically engineered myeloid cells rebalance the core immune suppression program in metastasis

Graphical abstract



Authors

Sabina Kaczanowska, Daniel W. Beury, Vishaka Gopalan, ..., Sridhar Hannenhalli, Michael C. Kelly, Rosandra N. Kaplan

Correspondence

rosie.kaplan@nih.gov

In brief

Genetically engineered myeloid cells expressing IL-12 can reverse the immunosuppressive environment developed during metastatic progression by augmenting T cell responses and reducing metastatic burden in preclinical models.

Highlights

- A myeloid-rich, T-cell-poor immunosuppressive microenvironment promotes metastasis
- Genetically engineered myeloid cells (GEMys) deliver IL-12 to metastatic sites
- IL12-GEMys reverse immune suppression and activate anti-tumor immunity
- Chemotherapy with IL12-GEMy treatment achieves durable cures in pre-clinical models



Article

Genetically engineered myeloid cells rebalance the core immune suppression program in metastasis

Sabina Kaczanowska,^{1,4} Daniel W. Beury,^{1,4} Vishaka Gopalan,² Arielle K. Tycko,¹ Haiying Qin,¹ Miranda E. Clements,¹ Justin Drake,¹ Chiadika Nwanze,¹ Meera Murgai,¹ Zachary Rae,³ Wei Ju,¹ Katherine A. Alexander,¹ Jessica Kline,¹ Cristina F. Contreras,¹ Kristin M. Wessel,¹ Shil Patel,¹ Sridhar Hannenhalli,² Michael C. Kelly,³ and Rosandra N. Kaplan^{1,5,*}

¹Tumor Microenvironment and Metastasis Section, Pediatric Oncology Branch, Center for Cancer Research, National Cancer Institute, National Institutes of Health, 10 Center Drive, Bethesda, MD 20892, USA

²Cancer Data Science Laboratory, Center for Cancer Research, National Cancer Institute, National Institutes of Health, 10 Center Drive, Bethesda, MD 20892, USA

³Single Cell Analysis Facility, Center for Cancer Research, National Cancer Institute, National Institutes of Health, 37 Convent Drive, Bethesda, MD 20892, USA

⁴These authors contributed equally

⁵Lead contact

*Correspondence: rosie.kaplan@nih.gov

<https://doi.org/10.1016/j.cell.2021.02.048>

SUMMARY

Metastasis is the leading cause of cancer-related deaths, and greater knowledge of the metastatic microenvironment is necessary to effectively target this process. Microenvironmental changes occur at distant sites prior to clinically detectable metastatic disease; however, the key niche regulatory signals during metastatic progression remain poorly characterized. Here, we identify a core immune suppression gene signature in pre-metastatic niche formation that is expressed predominantly by myeloid cells. We target this immune suppression program by utilizing genetically engineered myeloid cells (GEMys) to deliver IL-12 to modulate the metastatic microenvironment. Our data demonstrate that IL12-GEMy treatment reverses immune suppression in the pre-metastatic niche by activating antigen presentation and T cell activation, resulting in reduced metastatic and primary tumor burden and improved survival of tumor-bearing mice. We demonstrate that IL12-GEMys can functionally modulate the core program of immune suppression in the pre-metastatic niche to successfully rebalance the dysregulated metastatic microenvironment in cancer.

INTRODUCTION

Metastasis is the leading cause of death in patients with extra-cranial solid tumors (Wiens and Hattab, 2014; Rove and Crawford, 2009; Svensson et al., 2017; Scully et al., 2012). Despite recent advances in cancer treatment, there is an unmet need to better understand the metastatic process, and the development of effective therapies for metastatic disease remains a major challenge. The metastatic microenvironment offers a potential therapeutic target given its vital role in the pathogenesis and regulation of metastasis (Joyce and Pollard, 2009; Psaila and Lyden, 2009; Paget, 1989). During cancer progression, the primary tumor secretes systemic factors that prime distant sites for metastasis (Peinado et al., 2012, 2017). The specialized microenvironment that is established at distant sites before clinically detectable metastasis that supports the seeding and outgrowth of disseminated cancer cells is termed the pre-metastatic niche (Paget, 1989; Kaplan et al., 2005; Giles et al., 2016; Murgai et al., 2017; Liu and Cao, 2016; Welch and Hurst, 2019; Liu et al., 2016; Gui et al., 2020; Kaczanowska and Kaplan, 2020). The pre-metastatic niche is a complex and dynamic

microenvironment, with tumor-derived factors triggering the activation of non-immune stromal cells, extracellular matrix remodeling, and accumulation of bone-marrow-derived cells (Kaplan et al., 2005; Murgai et al., 2017; Giles et al., 2016). We have previously shown the expansion of hematopoietic stem and progenitor cells in the bone marrow of tumor-bearing mice, with these cells entering circulation and arriving in pre-metastatic lungs prior to the arrival of tumor cells (Kaplan et al., 2005; Giles et al., 2016). Elevated circulating progenitor cells can also be detected in cancer patients at diagnosis and are predictive of disease relapse (Giles et al., 2016). These circulating progenitor cells enter the pre-metastatic lung where they differentiate into immunosuppressive myeloid cells (Giles et al., 2016). Therefore, we hypothesize that myeloid-mediated immune suppression is a central regulator of metastasis.

To expand on our observations that bone-marrow-derived myeloid cells accumulate in pre-metastatic lungs, we set out to explore the function of these cells in the pre-metastatic niche and interrogate changes in the immune compartment in pre-metastatic lungs during the course of tumor progression. Myeloid cells can limit T cell activation and intravasation



(Gabrilovich et al., 2012; Davidson et al., 2017), provide cues to induce regulatory T cells (Park et al., 2018; Fujimura et al., 2012), and are a frequent component of many tissue-specific stem cell niches (Naik et al., 2018; Wang et al., 2019a; Rahmani et al., 2018; Sehgal et al., 2018; Ko et al., 2017; Mussar et al., 2017). These myeloid-based immuno suppressive mechanisms are also well characterized in the context of tumorigenesis and in the primary tumor microenvironment (Gabrilovich, 2017; Gabrilovich et al., 2012; Kumar et al., 2016; Qian et al., 2009; Veglia et al., 2019; Albrengues et al., 2018). Therefore, we reason that the immune regulation that tightly governs stem cell niche biology might also be relevant to the niche that fosters metastatic progression.

Here, we comprehensively explore the dynamics of immune cells in the earliest metastatic microenvironment of the lung and interrogate the core niche programs by transcriptional profiling of the pre-metastatic lungs of tumor-bearing mice. We utilized multi-dimensional flow cytometry, high-resolution tissue RNA sequencing (RNA-seq), and single-cell RNA sequencing (scRNA-seq) to define how metastatic progression reshapes the immune landscape within the lung. Our findings reveal that myeloid cell signatures and pathways are among the most significantly enhanced features of the pre-metastatic microenvironment of the lung and that the transcriptional profile of the pre-metastatic niche is enriched in an immune suppression gene signature derived predominantly from myeloid populations. We hypothesize that reprogramming myeloid-mediated immune suppression pathways in the pre-metastatic microenvironment could limit metastatic disease.

In order to determine the impact of disrupting immune suppression in the pre-metastatic niche, we investigate the use of myeloid cells as a platform to deliver antitumor cytokines to pre-metastatic sites. To take advantage of the accumulation of myeloid cells that help create the pre-metastatic niche, we generated genetically engineered myeloid cells (GEMs) to deliver the antitumor cytokine interleukin-12 (IL-12) into the local milieu during metastatic progression. IL-12 is produced by myeloid cells in response to infection and cancer, stimulates T and natural killer (NK) cell priming, effector function, and survival, and induces a strong interferon gamma (IFN- γ) response that increases antigen presentation and decreases pro-tumorigenic processes such as angiogenesis and extracellular matrix remodeling (Brunda et al., 1993; Colombo and Trinchieri, 2002; Del Vecchio et al., 2007; Steding et al., 2011; Strauss et al., 2019). Previous efforts to use IL-12 clinically through systemic administration or secretion by T cells have had limitations due to toxicity associated with the presence of high levels of systemic IL-12, highlighting the need to mimic a more physiologic approach for the local delivery of IL-12 (Kerkar et al., 2011; Zhang et al., 2011, 2015). Other groups have utilized macrophages or dendritic cells to secrete therapeutic factors into tissue sites; however, these terminally differentiated cells have different functional properties and have not been investigated in metastatic disease (Moyes et al., 2017; Tatsumi et al., 2003; Klichinsky et al., 2020). Based on the unique homing and surveillance properties of myeloid cells that lead to their accumulation in pre-metastatic sites, myeloid cells have the capability to infiltrate even immunologically “cold” tumors where T cells are often excluded

or limited to the periphery (Awad et al., 2018). Harnessing the homing and tumorotropic properties of myeloid cells for the local delivery of specific cargo is a promising therapeutic strategy for the treatment of cancer and metastasis.

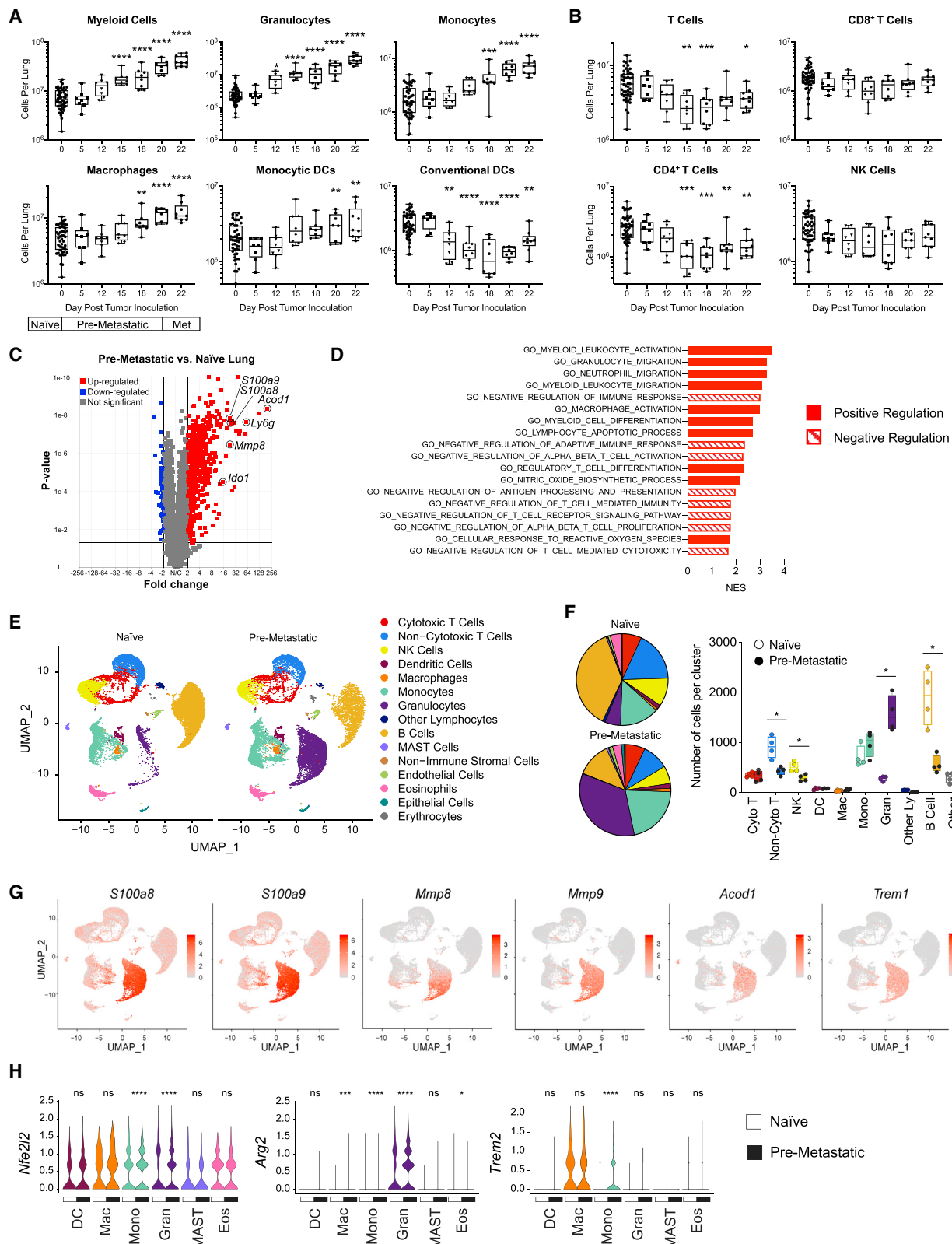
Transcriptomic analysis of lung tissue following administration of IL-12-secreting GEMs (IL12-GEMs) demonstrates a dramatic reprogramming of the metastatic niche, resulting in down-regulation of immunosuppressive pathways, upregulation of antigen presentation machinery, and subsequent activation of cytotoxic T cell and NK cell responses. Treatment of mice bearing established tumors with IL12-GEMy therapy significantly reduced metastatic and primary tumor burden, prolonging the survival of mice in an IL-12- and T cell-dependent manner. Our study sheds light on how myeloid cells, one of the most abundantly recruited populations to tumor and metastatic microenvironments, can be harnessed as a platform to locally deliver cargo to rebalance dysregulated microenvironments.

RESULTS

Immune characterization of the pre-metastatic microenvironment identifies a core regulatory transcriptional program of myeloid-mediated immune suppression

We aimed to explore how immune populations change in the lung in response to primary tumor growth at a distant site. We utilized M3-9-M, a syngeneic orthotopic tumor model of rhabdomyosarcoma, that spontaneously metastasizes to the lungs and is highly analogous to human metastatic rhabdomyosarcoma (Meadors et al., 2011), an aggressive pediatric cancer arising from muscle tissue. We examined immune population dynamics in the lungs of tumor-bearing mice by flow cytometry (Figures 1A and 1B) at pre- (days 5–20) and early (~days 20–22) metastatic time points (Figures S1A–S1E). We define the pre-metastatic window as the time points during primary tumor progression prior to evidence of metastasis in the lung by visual inspection, flow cytometry (Figure S1B), or bioluminescent imaging of labeled tumor (Giles et al., 2016), not excluding the possible presence of disseminated tumor cells or very early micro-metastasis (Murgai et al., 2017; Kaplan et al., 2005). We observed a significant increase in the number of myeloid cell populations, including granulocytes, monocytes, macrophages, and monocytic dendritic cells (DCs) in the lungs of tumor-bearing mice (Figure 1A). Conversely, we found a dramatic decrease of conventional DCs, which are needed for antigen presentation and priming of an effective adaptive immune response.

In parallel, we discovered that there is a marked reduction in the number of T cells in pre-metastatic lungs, primarily in the CD4 $^{+}$ T cell compartment, while the number of CD8 $^{+}$ T cells and NK cells were not significantly changed (Figure 1B). Furthermore, we found that PD1 $^{\text{hi}}$ CD44 $^{\text{int}}$ T cells, associated with a dysfunctional phenotype, are most significantly increased in the pre-metastatic lung (Figure S1E) (Xia et al., 2019). Although T cell numbers are diminished in pre-metastatic lungs, both CD4 $^{+}$ and CD8 $^{+}$ T cells retain their proliferative capacity when isolated from the pre-metastatic microenvironment and activated with CD3/CD28 beads *in vitro* (Figure S1F), suggesting that local signals within the pre-metastatic milieu suppress



(legend on next page)

T cell activity rather than an intrinsic defect in T cell expansion. These data demonstrate the presence of a myeloid-rich, T cell-poor microenvironment that is formed in pre-metastatic lungs during cancer progression.

In order to investigate the transcriptional programs that underlie the pre-metastatic niche environment, we performed deep transcriptional analysis of whole lungs from naive and pre-metastatic mice. We found a dramatic shift in the expression of many genes in the lungs in response to the presence of a distant tumor (Figure 1C; Figures S2A and S2B). Genes associated with adaptive immune cell recruitment and activation (*Cxcl9*, *Tarm1*, *Ifng*, *Gzmb*) are significantly increased in tumor-bearing mice compared to naive mice, demonstrating an activated immune response in the lung during the pre-metastatic phase (Figure S2C). Most notably, we identified many upregulated genes associated with immune suppression (*Acod1*, *Ly6g*, *S100a8*, *S100a9*, *Mmp8*, *Mmp9*, *Ido1*, *Trem1*, *Il1b*, *Arg1*) (Figure S2C). These data provide evidence that the pre-metastatic lung does not lack adaptive immunity, but rather there is a program of active immune suppression that inhibits effective antitumor immunity. To better define this program of immune suppression, we created a pre-metastatic gene signature based on the top 50 genes upregulated and downregulated in pre-metastatic compared to naive lungs (Figure S2C). We compared this signature to published datasets and found that the genes upregulated in the lung pre-metastatic niche in our rhabdomyosarcoma model are conserved in pre-metastatic sites in other metastatic tumor models (Figure S2D) (Hiratsuka et al., 2008; Liu et al., 2016; Shao et al., 2018; Yamamoto et al., 2008; Lee et al., 2019).

To investigate the functional implications of this drastic change in gene expression between pre-metastatic and naive lungs, we performed gene set enrichment analysis (GSEA). We identified the enrichment of gene ontology (GO) gene sets associated with myeloid cell activation, migration, and differentiation in parallel with negative regulation of adaptive and T cell-mediated immune responses (Figure 1D). Ingenuity pathway analysis (IPA) indicated a significant enrichment in multiple pathways of myeloid cell-mediated immune suppression, including production of nitric oxide (NO) and reactive oxygen species (ROS), p38 MAPK signaling, granulocyte-macrophage colony-stimulating factor (GM-CSF) signaling, the inflammasome pathway,

and inducible nitric oxide synthase (iNOS) signaling (Figure S2E) (Gabrilovich, 2017; Yang et al., 2010; Wang et al., 2006; Hong, 2016; Guo et al., 2016; Cao and Xu, 2019; Wang et al., 2019b; Gui et al., 2020). T cell exhaustion-associated pathways are also enriched in the pre-metastatic lungs (Figure S2E), and genes associated with a functional T cell response were downregulated in the pre-metastatic setting such as *IL12a*, *Tril*, and *Ccr6* (Figure S2C), implicating active suppression of adaptive immune responses during metastatic development. Furthermore, liver X receptor (LXR)/retinoid X receptor (RXR) and peroxisome proliferator-activated receptor (PPAR) signaling are significantly downregulated in the lungs of tumor-bearing mice, which are pathways involved in lipid metabolism, suppression of tumor growth, reduction of myeloid-derived suppressor cell abundance, and dampening inflammation in the bone-marrow niche (Figure S2E) (Tavazoie et al., 2018; Noelia and Castrillo, 2011; Hong et al., 2012; Croasdell et al., 2015; Casanova-Acebes et al., 2014). Further, we performed functional annotation analysis of the top 50 genes upregulated in pre-metastatic lungs that confirmed the significant enrichment of many myeloid-mediated biological processes that play a role in immune suppression (Figure S2F). Among these, leukocyte and neutrophil migration and aggregation indicate enhanced expression of genes that promote the intravasation of myeloid cells early in metastatic progression, while NO and ROS biosynthesis and protein nitrosylation demonstrate inhibition of T cell receptor signaling and attenuated T cell activation (Figure S2F) (Gabrilovich, 2017; Nagaraj et al., 2007). Together, our transcriptomics data support a core module of immune suppression within the pre-metastatic niche.

To further elucidate the cellular source of the transcriptional immune suppression program in the lungs of tumor-bearing hosts, we performed scRNA-seq of naive and pre-metastatic lungs. Cell-type identity of each cluster was defined by the expression of lineage markers (Figures S3A and S3B). scRNA-seq revealed a global shift in immune cell populations (Figure 1E). Consistent with our flow cytometry data, we observed a striking expansion of the number of granulocytes along with a significant decrease in lymphocytes including non-cytotoxic T cells, NK cells, and B cells compared to naive lung (Figure 1F). Key immune suppression genes from the pre-metastatic niche gene

Figure 1. Immune cell populations are dysregulated and upregulate a core immune suppression gene signature in the pre-metastatic lung
(A and B) Lungs from M3-9-M ffluc-eGFP tumor-bearing mice were harvested at various time points ($n = 8$) and processed into single-cell suspension. Naive mice were taken at each time point and are indicated as day 0 post-tumor inoculation. Flow cytometry analysis of (A) myeloid populations (myeloid = CD11b⁺, granulocytes = CD11b⁺Ly6G⁺, monocytes = CD11b⁺Ly6G⁻Ly6C⁺, macrophages = CD11b⁺F4/80⁺, monocytic dendritic cells = CD11b⁺CD11c⁺, conventional dendritic cells = CD11b⁻CD11c⁺) and (B) lymphocyte populations (T cells = CD3⁺, CD8⁺ T cells = CD3⁺CD8⁺, CD4⁺ T cells = CD3⁺CD4⁺, NK cells = CD3⁻NK1.1⁺). All populations are gated on live CD45⁺ single cells. Data were analyzed by ordinary one-way ANOVA with Dunnett's multiple comparisons test between the mean of day 0 and each time point.

(C and D) Lungs were harvested from naive mice or on day 15 post-primary tumor inoculation and flash frozen, and RNA was isolated for bulk mRNA sequencing ($n = 4$). Data are presented as (C) a volcano plot and (D) select gene sets that were significantly enriched ($q < 0.1$) in RNA-seq expression profiles of pre-metastatic compared to naive lungs.

(E-H) Lungs were harvested from naive mice or on day 15 post-primary tumor inoculation and processed into single-cell suspension for scRNA-seq ($n = 4$). (E) UMAP plots of cell clusters. (F) Pie charts and plot of cell number per cluster analyzed by the Kolmogorov-Smirnov test. (G) Feature plots showing the expression level of select genes from the pre-metastatic gene signature across the cell clusters. (H) Expression levels of select genes in myeloid cell clusters. Statistical differences between groups were analyzed by the Wilcoxon test.

DC, dendritic cells; Mac, macrophages; Mono, monocytes; Gran, granulocytes; MAST, MAST cells; Eos, eosinophils. *** $p < 0.0001$; ** $0.0001 < p < 0.001$; ** $0.001 < p < 0.01$; * $0.01 < p < 0.05$. In boxplots, the center line represents the median, the box limits denote the 25th to the 75th percentile, and the whiskers represent the minimum and maximum value. See also Figures S1, S2, S3, and S4.

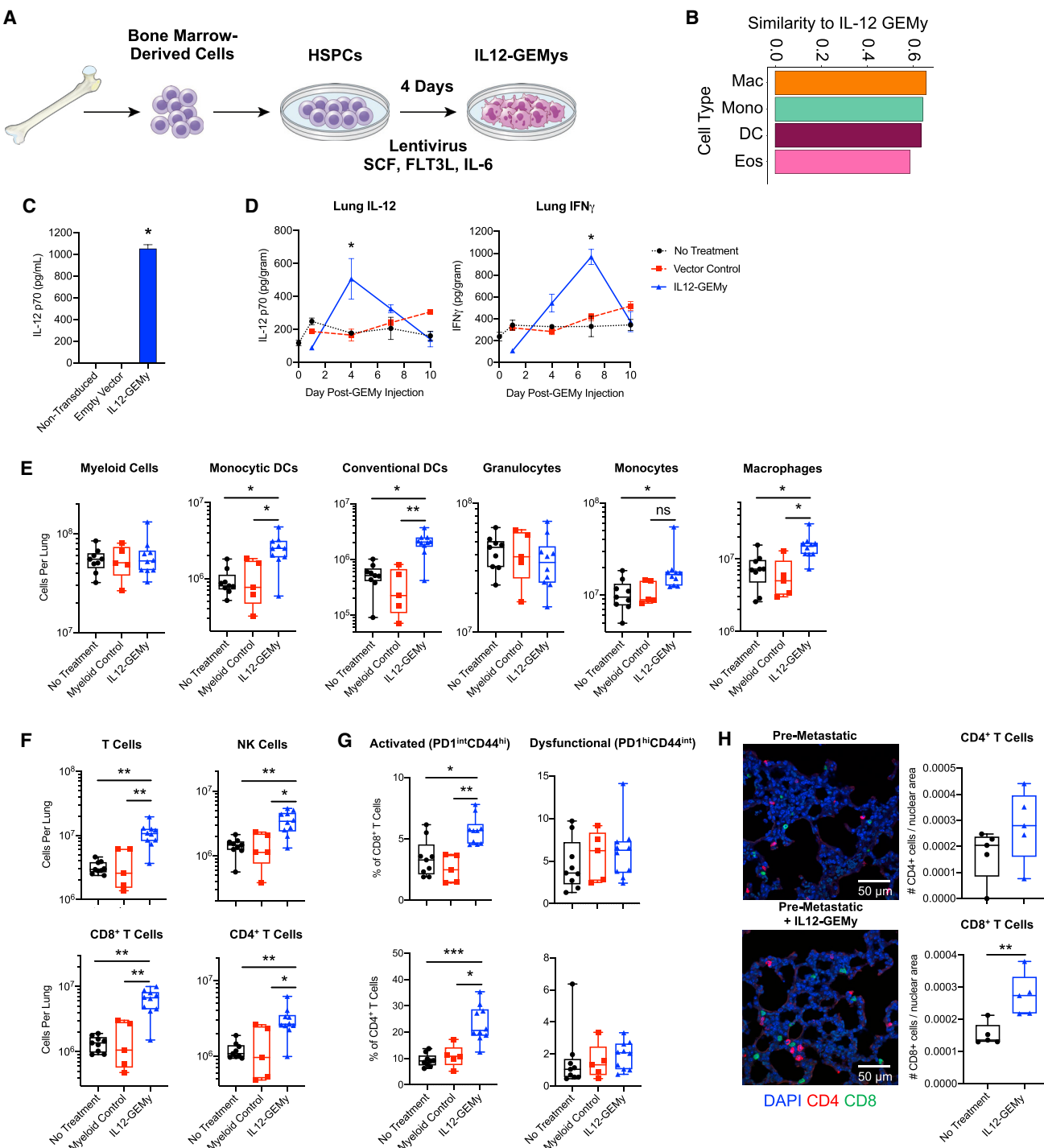


Figure 2. IL12-GEMy treatment alters immune populations in pre-metastatic lungs

(A) Schematic of IL12-GEMy production.

(B) Cosine similarity of IL12-GEMy bulk RNA-seq data with profiles of each cluster in scRNA-seq data. Similarity is based on the expression of the most variable genes in randomly drawn sub-samples of 90% of cells in each cluster. The similarity score was then computed as the average cosine similarity across 100 sub-samples and the IL12-GEMy product. The similarity score can range between 0 and 1, indicating either complete dissimilarity or similarity, respectively, with 0.65 being the highest score in our data. The four most similar populations to IL12-GEMys are shown.

(C) IL12-GEMys were washed after transduction, plated at 5×10^5 cells/mL, and cultured for 18 h. Supernatant was collected and analyzed for IL-12 by ELISA. Statistical significance was calculated using the Kruskal-Wallis test.

(legend continued on next page)

signature (Figure S2C) are most highly expressed by myeloid cells, including *S100a8*, *S100a9*, *Mmp8*, *Mmp9*, *Acod1*, and *Trem1* (Figure 1G; Figure S3C). In addition, *Nfe2l2*, *Arg2*, and *Trem2*, genes implicated in the immunosuppressive function of myeloid cells, are upregulated by many myeloid cell types in the pre-metastatic niche (Figure 1H) (Beury et al., 2016; Grzywa et al., 2020; Katzenellenbogen et al., 2020).

Furthermore, evolutionarily conserved interferon-inducible transmembrane genes that play a role in suppressing interferon-mediated immunity in stem cell niches, *Ifitm1* and *Ifitm3*, were also significantly upregulated in myeloid populations in the pre-metastatic lungs (Figure S3D). We found a high degree of similarity between many of the myeloid-associated immune suppression genes that we found in our sequencing data and human bone-marrow myeloid populations from the hematopoietic stem cell niche (*TREM1*, *CYBB*, *S100A8*, *S100A9*, *IL1B*, *IFITM1*, *IFITM3*) (Figure S4) (Hay et al., 2018), drawing a parallel between the programs limiting immune responses in the pre-metastatic niche and stem cell niche.

These data demonstrate that the pre-metastatic niche is a myeloid-rich, T cell-poor microenvironment expressing a core regulatory program of active myeloid-mediated immune suppression.

Generation of genetically engineered myeloid cells to locally deliver immunomodulatory cargo into the pre-metastatic microenvironment

We and others have shown that bone-marrow-derived myeloid cells are elevated in circulation and highly enriched in the tumor and metastatic microenvironments in both mice and humans (Figure 1) (Giles et al., 2016; Pollard, 2004; Zhang et al., 2016; Teng et al., 2015). To take advantage of this marked infiltration of myeloid cells into pre-metastatic lungs, we generated genetically engineered myeloid cells, herein referred to as “GEMys,” as an immunotherapy platform to deliver cargo to manipulate the microenvironment of the pre-metastatic niche. As IL-12 has previously been shown to demonstrate potent antitumor activity (Wolf et al., 1991; Brunda et al., 1993; Colombo and Trinchieri, 2002), we designed GEMys to secrete IL-12 (IL12-GEMys) to target the core immune suppression program in the metastatic microenvironment. Given that the myeloid cells accumulating in the pre-metastatic lungs are of bone-marrow origin (Giles et al., 2016), we generated GEMys from lineage-depleted bone-marrow hematopoietic stem and progenitor cells (HSPCs). Cells were transduced

with lentivirus encoding IL-12 and the Thy1.1 reporter, and cultured in the presence of SCF, FLT3L, and IL-6 for 4 days (Figure 2A). The IL12-GEMy product is a heterogeneous population, predominantly resembling the macrophage and monocyte profiles within our scRNA-seq clusters (Figure 2B), with a large component of Ly6G⁻Ly6C⁺ monocytes (Figure S5A). IL-12 production was confirmed by ELISA (Figure 2C; Figure S5B).

Upon intravenous (i.v.) administration of IL12-GEMys into tumor-bearing mice, IL-12 levels peaked in the lungs at 4 days post-treatment, followed by a delayed peak of IFN-γ production at 1 week (Figure 2D). Similar trends were seen in the serum, spleen, and tumor, with no appreciable differences in IL-12 or IFN-γ in the liver over vector-control-treated mice (Figure S5C). Notably, the highest IFN-γ levels were detected in the lung and in the tumor, at levels two times greater than the amount detected in the serum and spleen (Figure 2D; Figure S5C). IL12-GEMys generated from CD45.1⁺ Pepboy mice transferred into CD45.2⁺ wild-type hosts were detected primarily in the lung, liver, and spleen in similar proportions as vector-control cells at 24 h after adoptive transfer, suggesting that the expression of IL-12 does not significantly impact cell homing (Figure S5D). Both IL12-GEMy and vector-control cells were detected at low frequencies in the bone marrow, tumor, lymph nodes, and blood. In contrast to the high proportion of Ly6G⁺ endogenous myeloid cells, IL12-GEMys retain a Ly6G⁻ monocytic phenotype in the lungs, suggesting that their phenotype is not drastically changed upon injection *in vivo* (Figure S5E). Together these data demonstrate the feasibility of generating functional murine GEMys from HSPCs and that IL12-GEMys effectively deliver IL-12 to the pre-metastatic microenvironment.

IL12-GEMys restore and activate T cell populations in pre-metastatic lungs

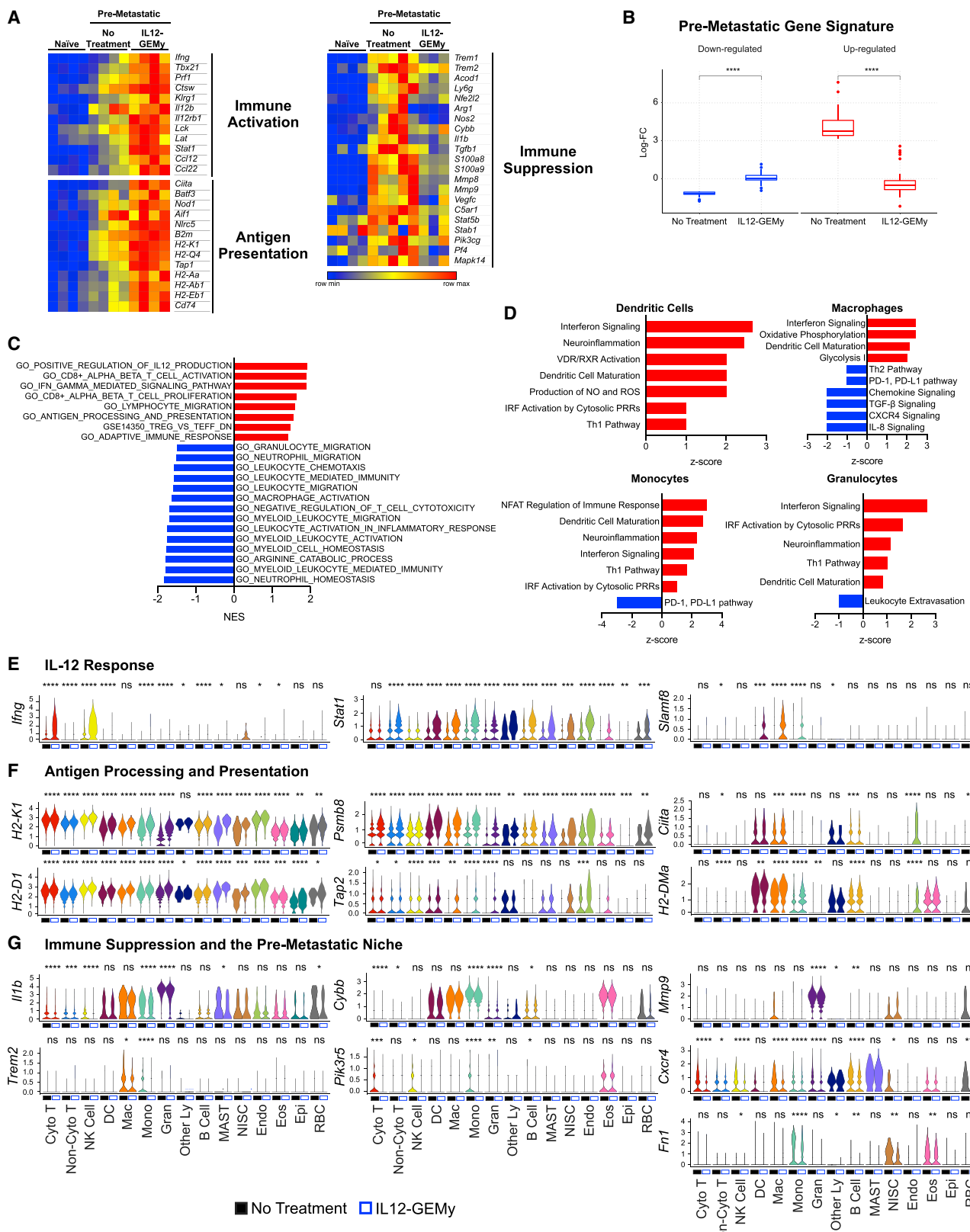
To determine the impact of IL12-GEMys on immune populations in the metastatic microenvironment, we profiled lymphoid and myeloid populations in the lungs of mice at primary tumor endpoint that received either no treatment, control myeloid cells, or IL12-GEMys. Although, there was no significant change in the total number of myeloid cells in the lungs of IL12-GEMy-treated mice compared to controls, there was a significantly higher number of both monocytic and conventional DCs, which can serve as professional antigen-presenting cells to activate adaptive immunity, along with monocytes and macrophages (Figure 2E).

(D) 8×10^6 vector control or IL12-GEMys generated from GFP⁺/Luciferase⁺ donor mice were injected into M3-9-M tumor-bearing mice 12 days after primary tumor inoculation (n = 3–6 mice per group per time point). Lungs were harvested and flash frozen at indicated time points, and tissues were homogenized and analyzed by ELISA. Statistical analysis was performed by the Kolmogorov-Smirnov test at each time point.

(E–G) Mice were inoculated with M3-9-M ffuc-mCherry tumor and not treated (n = 9) or treated with control non-transduced myeloid cells (n = 5) or IL12-GEMys (n = 10) on days 12, 19, and 26. Lungs were harvested on day 27 and analyzed by flow cytometry gated on live CD45⁺ single cells. Flow cytometry data were analyzed by the Kruskal-Wallis test with Dunn’s multiple comparisons test. (E) Myeloid cell populations in the lungs (myeloid = CD11b⁺, monocytic dendritic cells = CD11b⁺CD11c⁺, conventional dendritic cells = CD11b⁺CD11c⁺, granulocytes = CD11b⁺Ly6G⁺, monocytes = CD11b⁺CD43⁺Ly6C⁺, macrophages = CD11b⁺CD43⁺Ly6C⁺F4/80⁺). (F) The number of T and NK cells in the lungs (T cells = CD3⁺, CD8⁺ T cells = CD3⁺CD8⁺, CD4⁺ T cells = CD3⁺CD4⁺, NK cells = CD3⁻NK1.1⁺). (G) The proportion of CD8⁺ and CD4⁺ T cells expressing PD1 and CD44 in the lungs.

(H) Immunofluorescence staining of FFPE lung sections collected 15 days after tumor inoculation, 3 days after treatment with 8×10^6 IL12-GEMys. Quantification was performed on 20 \times images of n = 5 mice per group, 8 images per mouse, and analyzed by the Kolmogorov-Smirnov test. Representative 40 \times images of nuclear (blue), CD4 (red), and CD8 (green) staining is shown.

Scale bar represents 50 μ m. ****p < 0.0001; ***0.0001 < p < 0.001; **0.001 < p < 0.01; *0.01 < p < 0.05. In bar and line graphs, data are represented as mean \pm SEM. In boxplots, the center line represents the median, the box limits denote the 25th to the 75th percentile, and the whiskers represent the minimum and maximum value. See also Figure S5.



(legend on next page)

Dendritic cells increased in the lung as early as 1 week following IL12-GEMy treatment, while other myeloid populations remained relatively stable (Figure S5F). There were minimal changes in myeloid populations in the spleen, lymph nodes, and tumor between IL12-GEMy-treated and control mice (Figure S5G).

The lungs of tumor-bearing mice that received IL12-GEMys had significantly more CD8⁺ T cells, CD4⁺ T cells, and NK cells compared to mice receiving no treatment or control myeloid cells (Figure 2F). Additionally, IL12-GEMy treatment significantly increased the relative percentage of activated PD1^{int}CD44^{hi} T cells without impacting the dysfunctional PD1^{hi}CD44^{int} T cell subset (Figure 2G). The increase of T cells 3 days after IL12-GEMy treatment was also observed by immunofluorescence imaging of lung tissue, which showed an increased trend in CD4⁺ cells and significantly higher numbers of CD8⁺ cells (Figure 2H). To further delineate the kinetics of T cell recruitment or expansion, lungs were harvested from M3-9-M tumor-bearing mice that were treated with IL12-GEMys and analyzed by flow cytometry at various time points. The number of T cells and NK cells increased as early as 3 days post-IL12-GEMy transfer (Figure S5H), while the greatest increase in the proportion of PD-1⁺ and CD44^{hi} T cells occurred between 3–7 days after IL12-GEMy delivery (Figure S5I), coinciding with IL-12 cargo delivery to the pre-metastatic lung and rise in IFN- γ levels (Figure 2D). There were no appreciable differences in the frequency of CD3⁺ and NK1.1⁺ cells in the spleen or tumor, with decreased NK1.1⁺ cells in the tumor-draining lymph node of IL12-GEMy-treated mice (Figure S5J), indicating a metastatic niche-specific response to IL12-GEMy treatment in tumor-bearing mice.

The IL12-GEMy cell number remained stable in the lung up to a week after transfer, indicating that the IL12-GEMys have limited expansion *in vivo* (Figure S5K). The proliferation of T cells expressing high levels of IL-12 was responsible for toxicity observed in previous studies (Obstfeld et al., 2017; Maude et al., 2014).

These data indicate that IL12-GEMy treatment reshapes the metastatic environment by promoting the accumulation of activated T cells, NK cells, and DCs in the lung.

IL12-GEMys reverse the core immune suppression program in the pre-metastatic lung

To determine the impact of IL12-GEMy treatment on the pre-metastatic microenvironment, we profiled the transcriptomic

landscape of the pre-metastatic lungs 3 days after treatment with IL12-GEMys. IL12-GEMy treatment promotes a dramatic shift in the transcriptional program of pre-metastatic lungs (Figures S6A and S6B). IL12-GEMy treatment induces the expression of genes associated with adaptive immune cell activation, such as Th1 phenotype (*Tbx21*, *Ifng*, *Stat1*), cytotoxicity (*Prf1*, *Ctsw*, *Klrg1*), and T cell receptor signaling (*Lck*, *Lat*) (Figure 3A). Furthermore, there is a dramatic upregulation of genes associated with antigen processing and presentation (*Ciita*, *Batf3*, *B2m*, *Tap1*, *H2-K1*, *H2-Q4*, *H2-Aa*, *H2-Ab1*, and *H2-Eb1*) (Figure 3A). Strikingly, immunosuppressive genes that are upregulated in pre-metastatic lungs compared to naive lungs are downregulated with IL12-GEMy treatment (Figure 3A). This reversal of the core immune suppression program is demonstrated by analyzing the pre-metastatic gene signature generated in Figure S2C. The top 50 genes downregulated in the pre-metastatic niche are significantly increased with IL12-GEMy treatment, and the top 50 genes upregulated in the pre-metastatic niche are significantly reduced with IL12-GEMy treatment (Figure 3B). This reversal of the core immune suppression program illustrates the plasticity of the pre-metastatic niche phenotype that can be targeted by the introduction of IL12-GEMys to induce profound reprogramming of the niche environment in the lungs of tumor-bearing mice.

GSEA confirmed the enrichment of gene sets associated with IL-12 production, CD8⁺ T cell activation, IFN- γ signaling, and antigen processing and presentation, together with the downregulation of gene sets related to myeloid cell homeostasis and migration (Figure 3C). Pathway analysis revealed the upregulation of T cell pathways related to antitumor activity, such as ICOS signaling (Hutloff et al., 1999; Soldevilla et al., 2019), PPAR signaling (Koeffler, 2003), Th1 activation, NFAT signaling, and interferon signaling (Figure S6C). In parallel, the transcriptional profile of IL12-GEMy-treated lungs revealed a significant downregulation of pathways involved in niche-associated immune suppression such as TGF- β , IL-1, IL-6, and iNOS signaling, as well as oxidative stress response and the production of NO and ROS (Figure S6C).

In order to examine the transcriptional effects of IL12-GEMys on specific cell populations, we performed scRNA-seq analysis on pre-metastatic lungs from tumor-bearing non-treated and IL12-GEMy-treated mice. Although there was no significant

Figure 3. IL12-GEMy treatment reverses the core immune suppression gene program in the lung microenvironment and activates adaptive immunity

Mice were inoculated with M3-9-M fflic-mCherry primary tumor and treated with 8×10^6 IL12-GEMys on day 12. Lungs were flash frozen (A–C) or processed into single-cell suspension (D–G) 3 days post-treatment (n = 4 mice per group).

- (A) Expression of selected genes in the lung comparing naive non-treated tumor-bearing mice and IL12-GEMy-treated tumor-bearing mice.
- (B) Log-fold changes of the top 50 genes upregulated in pre-metastatic lungs (red) and the top 50 genes downregulated in pre-metastatic lungs (blue) in the lungs of non-treated and IL12-GEMy-treated tumor-bearing mice. p values were determined using a one-sided Wilcoxon rank-sum test.
- (C) Gene set enrichment analysis of differential gene-expression data from the lungs of IL12-GEMy-treated compared to non-treated mice. Red bars indicate a positive normalized enrichment score (NES), and blue bars indicate a negative normalized enrichment score (NES).
- (D) Ingenuity pathway analysis of the differential gene expression between IL12-GEMy-treated and non-treated pre-metastatic lungs for individual myeloid cell clusters by single-cell RNA sequencing. Red bars indicate positive Z scores and blue bars indicate negative Z scores.

(E–G) Expression levels of key genes associated with (E) response to IL-12, (F) antigen processing and presentation, and (G) immune suppression and the pre-metastatic niche are shown on a per-cluster basis for non-treated and IL12-GEMy-treated tumor-bearing mice. Statistical differences between groups analyzed by the Wilcoxon test.

Cyto T, cytotoxic T cells; non-cyto T, non-cytotoxic T cells; NK cells, natural killer cells; DC, dendritic cells; Mac, macrophages; Mono, monocytes; Gran, granulocytes; other Ly, other lymphocytes; MAST, MAST cells; NISC, non-immune stromal cells; Endo, endothelial cells; Eos, eosinophils; Epi, epithelial cells; RBC, erythrocytes. ***p < 0.0001; ** 0.0001 < p < 0.001; ** 0.001 < p < 0.01; * 0.01 < p < 0.05. See also Figures S6A–S6D.

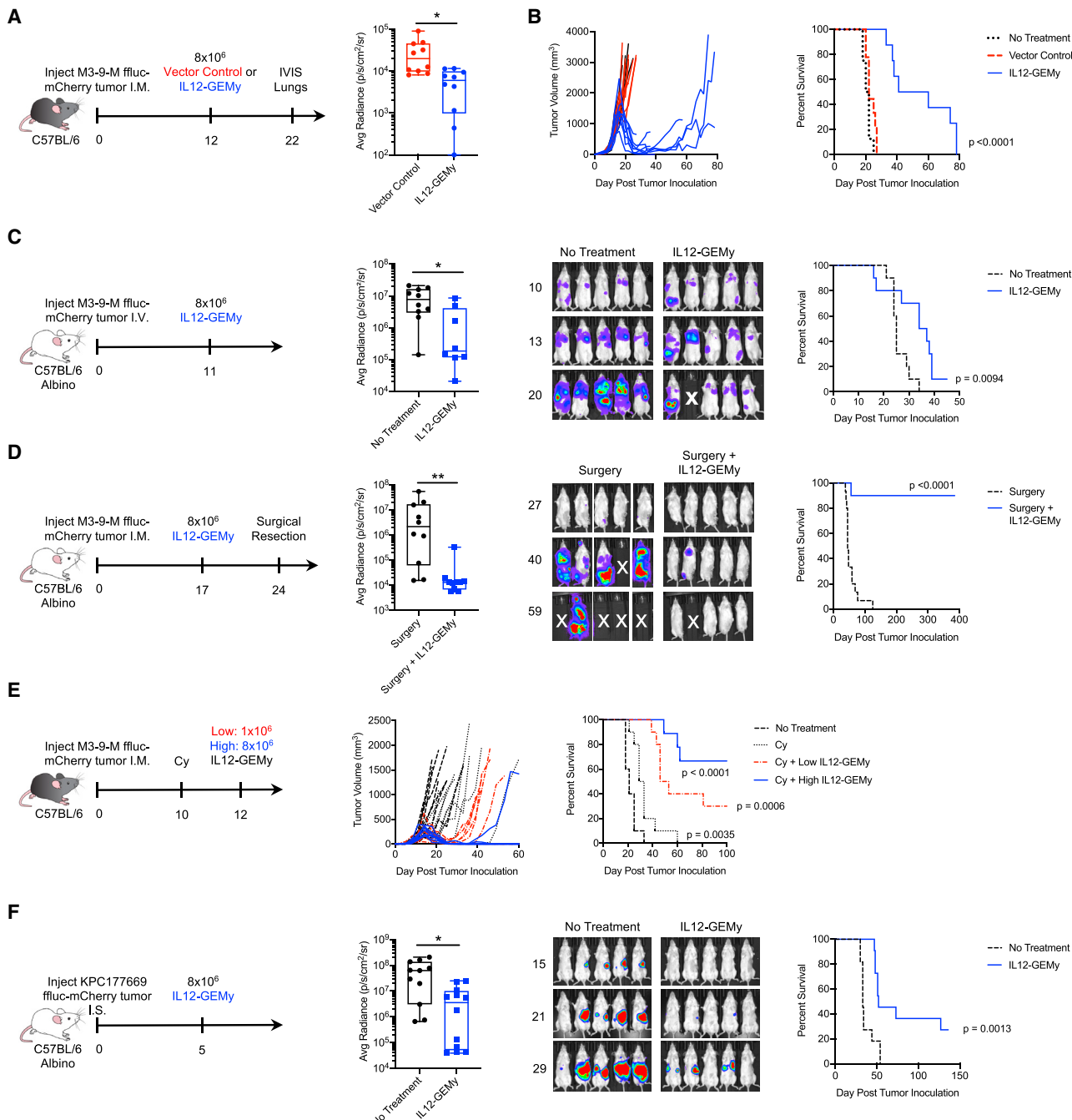


Figure 4. IL12-GEMy treatment limits metastasis and extends survival in mice

(A and B) Mice were injected orthotopically with 5 \times 10⁵ M3-9-M fflic-mCherry tumor cells and treated with 8 \times 10⁶ vector control or IL12-GEMys on day 12. (A) Lungs were harvested on day 22, and bioluminescent metastatic burden in the lungs was measured using an *in vivo* imaging system (IVIS) (n = 10 mice per group) and analyzed by the Kolmogorov-Smirnov test. (B) Mice were monitored for tumor growth and survival (n = 10 mice per group) analyzed by a log-rank (Mantel-Cox) test.

(C) Mice were injected with 5 \times 10⁴ M3-9-M fflic-mCherry via tail vein and treated with 8 \times 10⁶ IL12-GEMy i.v. 11 days post-tumor injection and then followed for survival and metastatic progression by bioluminescent imaging using IVIS (no treatment n = 10, IL12-GEMy n = 8). Quantification is shown on day 20 post-tumor inoculation and analyzed by a Kolmogorov-Smirnov test. Representative IVIS images and average radiance of tumor-bearing mice are shown. Survival curves were analyzed by a log-rank (Mantel-Cox) test.

(D) Mice were orthotopically injected with 5 \times 10⁵ M3-9-M fflic-mCherry cells and treated with 8 \times 10⁶ IL12-GEMys on day 17 followed by primary tumor resection by amputation of the tumor-bearing leg on day 24 and monitored for metastatic progression and survival by IVIS (no treatment n = 15, IL12-GEMy n = 10). Average radiance of mice on day 40 post-tumor injection analyzed by a Kolmogorov-Smirnov test, and representative IVIS images are shown.

(legend continued on next page)

change in the relative numbers of the myeloid cell populations by scRNA-seq, myeloid cells did demonstrate a marked shift of transcriptional reprogramming in response to IL12-GEMy (Figure S6D). To better understand IL12-GEMy-dependent phenotypic changes in the transcriptional programs of myeloid cells, we performed pathway analysis of myeloid cell clusters in the lungs of IL12-GEMy-treated versus non-treated tumor-bearing mice. We observed marked activation of interferon, Th1, and DC maturation pathways in monocytes, macrophages, granulocytes, and DCs (Figure 3D). In addition, there was also a strong reduction in genes related to leukocyte extravasation within the granulocyte population (Figure 3D). Notably, there was a strong downregulation of immunosuppressive pathways within myeloid clusters including the PD-1/PD-L1 axis, Th2 signaling, TGF- β , and IL-8 signaling (Figure 3D) (Gajewski et al., 2006). These findings implicate IL12-GEMy cell therapy in reducing a multitude of diverse signaling pathways within the pre-metastatic niche that can contribute to the core immune suppression program.

To further elucidate the contribution of specific cell types to the IL12-GEMy response, we examined the expression of relevant genes on a per cluster basis. One of the main downstream effects of IL-12 signaling is IFN- γ production, which is robustly induced after IL12-GEMy administration in cytotoxic T cells and NK cells, as well as significantly upregulated, although at a lower level, in DCs, monocytes, and granulocytes (Figure 3E). IFN- γ signals through Stat1, which is also highly upregulated by many cell types in the pre-metastatic niche in response to IL12-GEMys (Figure 3E). IFN- γ -induced Slamf8, a negative regulator of ROS production and migration in myeloid cells, is robustly upregulated in DCs, macrophages, and monocytes following IL12-GEMy treatment (Figure 3E) (Wang et al., 2015). IL-12 signaling is also associated with the upregulation of antigen presentation machinery (Kerkar et al., 2011). Many genes associated with both major histocompatibility complex (MHC) class I (*H2-K1*, *H2-D1*, *Psmb8*, *Tap2*) and MHC class II (*Ciita*, *H2-DMa*) antigen processing and presentation are dramatically upregulated in myeloid cells and many other cell types (Figure 3F). Furthermore, single-cell analysis revealed that the expression of many of the immunosuppressive genes is reduced in specific cell populations, such as *Il1b* (Mantovani et al., 2018) in monocytes and granulocytes, *Cybb* (Martner et al., 2019) in monocytes, and *Trem2* (Katzenellenbogen et al., 2020) in macrophages and monocytes (Figure 3G). Additionally, *Pik3r5*, a recently identified molecular switch that controls immune suppression (Kaneda et al., 2016), is reduced in cytotoxic T cell, NK cell, and monocyte populations (Figure 3G). Other genes that we and others have previously identified as playing vital roles in the pre-metastatic niche are also differentially regulated.

Mmp9 (Hiratsuka et al., 2002) is significantly downregulated in granulocytes and *Cxcr4*, an important chemokine receptor for HSPC homing (Giles et al., 2016), is reduced in many cell types (Figure 3G). Additionally, we and others have shown that perivascular cell-derived fibronectin (*Fn1*) is a key component of the pre-metastatic niche (Murgai et al., 2017; Kaplan et al., 2005; Psaila and Lyden, 2009; Høye and Erler, 2016). Here, we demonstrate that monocytes and eosinophils also contribute to fibronectin production in addition to non-immune stromal cells, and IL12-GEMy treatment significantly reduces *Fn1* production in all three populations (Figure 3G).

Together, these data provide evidence that IL12-GEMys have the ability to induce a cascade of transcriptional events in multiple cell types to reverse immune suppression in the pre-metastatic lung microenvironment, leading to the activation of adaptive immune responses. Further, our analysis offers key insights into the cell-specific responses to IL-12 signaling *in vivo* within the pre-metastatic niche environment.

IL12-GEMy treatment limits metastasis and improves survival

We next sought to determine whether reversing the core immune suppression signature in the pre-metastatic microenvironment with IL12-GEMy treatment has a therapeutic impact on metastatic disease progression. We utilized luciferase-expressing rhabdomyosarcoma tumor cells to measure spontaneous metastasis to the lung. Tumor-bearing mice were treated with vector control or IL12-GEMys, lungs were harvested on day 22, and bioluminescent signal was measured *ex vivo* for quantification of metastatic tumor burden. Mice treated with IL12-GEMys had significantly lower metastatic signal in their lungs than vector-control-treated mice (Figure 4A). IL12-GEMy-treated mice survived significantly longer than non-treated and vector-control-treated mice ($p < 0.001$), and we observed regression of established primary tumors (Figure 4B). As we did not observe a difference in tumor progression nor survival between vector-control and non-treated mice, we used non-treated mice as controls in future experiments.

To determine whether IL-12 delivery by GEMys is important or whether the presence of IL-12 in the myeloid cell culture results in therapeutic efficacy, we adoptively transferred control myeloid cells, *in vitro* IL-12 pre-treated myeloid cells, or IL12-GEMys into tumor-bearing mice. IL12-GEMy treatment significantly improved survival compared to non-treated mice ($p = 0.0006$) and had significantly smaller primary tumors at endpoint than mice without treatment or mice receiving non-transduced myeloid or IL-12 pre-treated myeloid cells (Figure S6E). Lungs from IL12-GEMy-treated mice had significantly less metastatic

(E) Mice were orthotopically inoculated with 5×10^5 M3-9-M fflic-mCherry cells. On day 10, groups of mice were left untreated or given a single dose of 2 mg cyclophosphamide (Cy) i.p. On day 12, groups of mice were left untreated or treated with 1×10^6 or 8×10^6 IL12-GEMys i.v. (labeled “low IL12-GEMy” and “high IL12-GEMy,” respectively) and followed for primary tumor growth and survival ($n = 10$). Statistics measured by a log-rank (Mantel-Cox) test are shown for Cy compared to no treatment ($p = 0.0035$), Cy + low IL12-GEMy compared to Cy ($p = 0.006$), and Cy + high IL12-GEMy compared to Cy ($p < 0.001$).

(F) Mice were injected intrasplenically with 5×10^5 KPC177669-fflic2-mCherry cells, spleens were resected, and mice were treated with 8×10^6 IL12-GEMys on day 5. Mice were monitored for survival and tumor growth by IVIS. Average radiance of tumor-bearing mice on day 29 analyzed by a Kolmogorov-Smirnov test, and representative IVIS images are shown (no treatment $n = 11$, IL12-GEMy $n = 12$). Survival data were tested for significance by a log-rank (Mantel-Cox) test. *** $p < 0.0001$; ** $0.0001 < p < 0.001$; ** $0.001 < p < 0.01$; * $0.01 < p < 0.05$. In boxplots, the center line represents the median, the box limits denote the 25th to the 75th percentile, and the whiskers represent the minimum and maximum value. See also Figures S6E–S6G.

burden and frequency of metastasis compared to lungs from non-treated mice (Figure S6F). By contrast, there was no significant difference in survival, primary tumor growth, or metastasis in mice that received either control or IL-12 pre-treated myeloid cells compared to mice without treatment (Figures S6E and S6F). Together these results demonstrate that the delivery of IL-12 by GEMys significantly reduces spontaneous metastasis and tumor progression in mice.

To evaluate the impact of IL12-GEMy treatment on metastatic tumors independent of primary tumor growth, mice were injected with tumor cells intravenously to establish lung lesions followed by IL12-GEMy treatment 11 days later and assessed for metastatic progression by bioluminescence imaging (Figure 4C). Mice treated with IL12-GEMys had decreased metastatic burden and increased survival, indicating that IL12-GEMys limit aggressive metastatic tumor growth.

Clinically, many rhabdomyosarcoma patients undergo surgical resection of their primary tumor; however, 30% of patients later relapse with metastatic disease (Pappo et al., 1999). In order to model neo-adjuvant treatment and metastasis independent of effects on primary tumor but in the presence of pre-metastatic niche formation, tumor-bearing mice were treated with IL12-GEMys followed by amputation of the tumor-bearing leg 1 week after treatment. A single dose of IL12-GEMy cell therapy prior to tumor resection significantly extended the survival of mice, with no evidence of disease over 1 year after treatment in 90% of mice, while all mice receiving surgery alone succumbed to relapsed disease (Figure 4D).

To determine whether the efficacy of IL12-GEMy treatment is dose dependent, we administered either a single high dose or low dose of IL12-GEMys to mice with established primary tumors (Figure S6G). Low-dose IL12-GEMys resulted in transient tumor regression in 20% of the mice with no significant improvement in survival, while high-dose IL12-GEMys resulted in more durable tumor regressions in 100% of mice, significantly enhancing the survival of mice relative to low-dose IL12-GEMys ($p = 0.0003$) (Figure S6G). These data indicate that the therapeutic efficacy of IL12-GEMys is dose dependent.

Many immunotherapies have demonstrated enhanced efficacy when used in combination with chemotherapy conditioning due to enhanced production of homeostatic chemokines and cytokines that occurs with chemotherapy-induced leukopenia (Turtle et al., 2016a; Heczey et al., 2017). Moreover, many T cell-based immunotherapies require chemotherapy preconditioning for optimal effect, leading us to ask whether the same might be true for myeloid cell-based therapies. To test whether the efficacy of IL12-GEMy therapy is enhanced by cyclophosphamide chemotherapy pre-conditioning, M3-9-M tumor-bearing mice were administered a single dose of 2 mg cyclophosphamide 10 days post-tumor inoculation followed by IL12-GEMy treatment 2 days later (Figure 4E). Cyclophosphamide alone had a modest delay in primary tumor growth and significantly increased survival compared to non-treated mice ($p = 0.0035$) (Figure 4E). The combination of cyclophosphamide with either low-dose or high-dose IL12-GEMys demonstrated a marked decrease in tumor progression and significantly improved survival compared to cyclophosphamide alone (Figure 4E). Furthermore, cyclophosphamide combined with IL12-

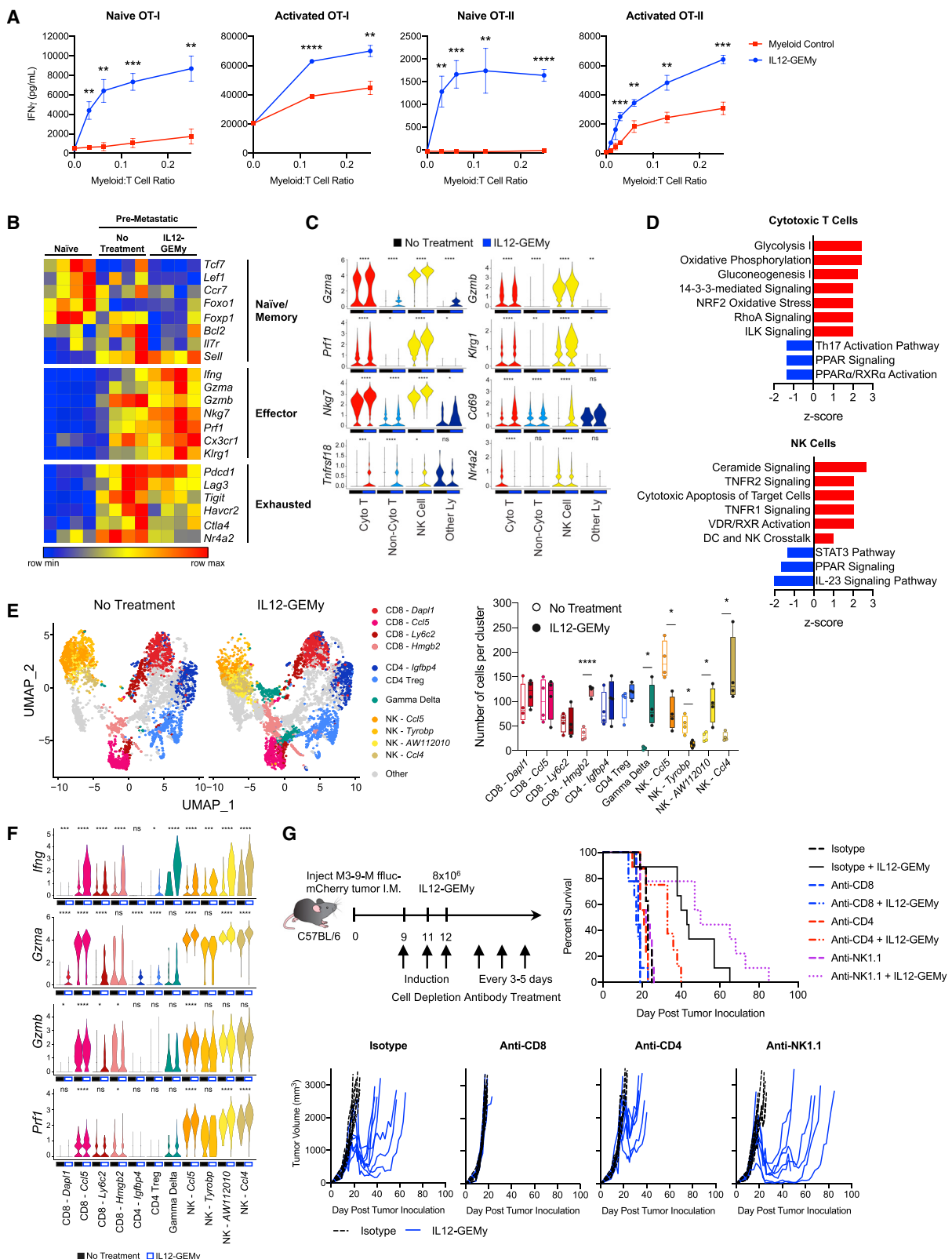
GEMy treatment was curative in 30% of mice receiving a low dose of IL12-GEMys and reached 66.7% in mice that received a high dose of IL12-GEMys (Figure 4E). These data indicate that the therapeutic benefit of chemotherapy pre-conditioning may be generalized to many types of cell-based immunotherapies and can greatly improve outcomes for IL12-GEMy therapy.

Given that IL12-GEMys can home to the liver (Figure S5D) and to extend our findings to an epithelial tumor model, we tested the impact of IL12-GEMy therapy on cancer progression in a highly aggressive pancreatic cancer liver metastasis model. KPC177669 is a *Kras^{-/-}/p53^{-/-}* tumor cell line derived from the KPC mouse model (Lee et al., 2016) that metastasizes specifically to the liver when cells are delivered into splenic circulation. Administration of IL12-GEMys 5 days post-intrasplicenic injection of tumor cells delayed primary tumor and metastatic outgrowth and significantly extended the survival of mice with KPC177669 pancreatic tumors ($p = 0.0013$) (Figure 4F). Together, these data indicate that IL12-GEMy therapy targets the metastatic process in multiple tumor models as well as the pre-metastatic niche of the liver. Our data demonstrate the therapeutic efficacy of the intravenous administration of a myeloid-based immunotherapy for the treatment of tumor progression and metastasis.

IL12-GEMy therapy activates T cell responses and is dependent on CD8⁺ T cells

Given the efficacy of IL12-GEMy therapy, we sought to further investigate the mechanism of action of IL12-GEMys in metastatic regulation. As pathways associated with T cell activation were upregulated in the lungs of IL12-GEMy-treated mice (Figure 3A), we more closely examined the mechanism of T cell activation by IL12-GEMys. Based on our findings of a strong *Ifng* gene signature in the transcriptomic analysis of whole lung (Figure 3A) and the induction of *Ifng* in the cytotoxic T cell cluster by single-cell analysis (Figure 3E), we evaluated the ability of IL12-GEMys to induce IFN- γ production by T cells. Co-culture of T cells with IL12-GEMys enhanced the ability of both naive and activated OT-I CD8⁺ and OT-II CD4⁺ T cells to produce IFN- γ *in vitro* in response to cognate peptide relative to co-culture with control myeloid cells (Figure 5A). These data demonstrate the direct impact that IL12-GEMys have on T cell IFN- γ -production and support our previous findings that IL12-GEMy function, at least in part, by inducing IFN- γ production by T cells *in vivo*.

Whole-lung deep transcriptomic profiling of IL12-GEMy-treated mice demonstrates low expression of genes associated with naive T cells and elevated expression of genes associated with effector function and cytotoxicity, suggesting that IL12-GEMy cell therapy promotes the activation of cytotoxic T cell responses (Figure 5B). Furthermore, the expression of genes associated with T cell exhaustion is low, suggesting that T cells are being functionally activated in the lungs of IL12-GEMy-treated mice (Figure 5B). Single-cell analysis demonstrates the upregulation of key cytotoxicity and activation markers in T cells and NK cells including *Gzma*, *Gzmb*, *Prf1*, *Klrg1*, *Nkg7*, *Cd69*, and *Tnfrsf18* (Figure 5C). Furthermore, expression of the T cell exhaustion regulator *Nr4a2* is significantly reduced in CD8⁺ and NK cells (Figure 5C) (Chen et al., 2019). Pathway analysis of the cytotoxic T cell cluster from scRNA-seq supports these



(legend on next page)

findings, as metabolic activity associated with T cell activation is significantly enriched in these cells (Figure 5D). Pathways related to NK cell activation, including ceramide signaling and cytotoxic apoptosis of target cells, are upregulated by IL12-GEMy treatment (Figure 5D). These data implicate cytotoxic T and NK cells as key effectors of IL12-GEMy cell therapy on limiting metastatic progression.

To gain a more detailed understanding of T and NK cell populations in the pre-metastatic niche following IL12-GEMy treatment, we selected the cytotoxic T cell, non-cytotoxic T cell, NK cell, and other lymphocyte clusters from our scRNA-seq analysis and performed higher resolution clustering analysis on these cell subsets (Figure 5E; Figure S6H). We observe a significant increase in CD8⁺ *Hmgb2*-expressing cells and gamma delta ($\gamma\delta$) T cells (Figure 5E). Interestingly, we found a decrease in NK cells expressing *Ccl5* and *Tyrobp* with an increase in NK cells expressing AW112020 and *Ccl4* (Figure 5E). Furthermore, we found that the *Ccl5*-expressing CD8⁺ T cell and NK cell clusters had the highest upregulation of *Ifng* and cytotoxic factors *Gzma*, *Gzmb*, and *Prf1* in response to IL12-GEMy treatment (Figure 5F). All of the NK cell clusters expressed these effector genes even in absence of treatment, which were further upregulated in the presence of IL-12 (Figure 5F). Of note, the $\gamma\delta$ T cell cluster significantly upregulated *Ifng* expression, which has been associated with the antitumor function of $\gamma\delta$ T cells (Schilbach et al., 2020) (Figure 5F). Together, these data provide insights into cell-specific responses to IL-12 in the pre-metastatic niche.

Given the robust activation of genes and pathways associated with T and NK cell function, we next tested which immune cell populations are necessary for the function of IL12-GEMys. We performed *in vivo* antibody depletion experiments to target CD8⁺, CD4⁺, or NK1.1⁺ cells to evaluate which lymphoid populations are necessary for mediating the efficacy of IL12-GEMy therapy (Figure 5G). Specific cell depletion was confirmed by flow cytometry of peripheral blood 1 week after initiation of the depletion antibody regimen (Figure S7A). IL12-GEMy treatment in the isotype-treated group reduced large established primary tumors and significantly extended survival ($p = 0.008$) of tumor-bearing mice (Figure 5G). Mice that were depleted of CD8⁺ cells

had no response to IL12-GEMy therapy, indicating that CD8⁺ cells are essential for the antitumor effect of IL12-GEMys. CD4⁺ cell targeting had a partial effect on IL12-GEMy efficacy, while depletion of NK1.1⁺ cells in combination with IL12-GEMy treatment did not have a significant difference in survival compared to the isotype plus IL12-GEMy treatment. These data demonstrate that CD8⁺ T cells play a critical role in the mechanism of action of IL12-GEMy therapy.

IL12-GEMy treatment enhances adoptive T cell therapy and generates long-lived immunological memory

Given that IL12-GEMy therapy is dependent on CD8⁺ T cells and promotes the activation of T cells *in vitro* and *in vivo*, we investigated the impact of IL12-GEMy therapy on the efficacy of adoptive T cell therapy. An ovalbumin (OVA)-expressing M3-9-M cell line was generated and confirmed to be recognized by CD8⁺ OT-I T cells (Figures S7B and S7C). OT-I T cells, IL12-GEMys, or a combination of the two were transferred into M3-9-M ffluc-mCherry-OVA tumor-bearing mice at sub-therapeutic doses of IL12-GEMys and T cells (Figure 6A). The transfer of low-dose OT-I T cells or IL12-GEMys alone did not impact primary tumor growth or survival. However, the combination of adoptive transfer of IL12-GEMys and OT-I T cells significantly increased the survival of the mice ($p < 0.0001$) and delayed primary tumor growth (Figure 6A). This enhancement of therapeutic activity was elicited in the absence of any pre-conditioning regimen, suggesting that the reversal of immune suppression with IL12-GEMy cell therapy was sufficient to enhance the antitumor activity of transferred T cells.

T cell therapies currently used in the clinic are given following a pre-conditioning regimen of cyclophosphamide and fludarabine (Cy/Flu) (Heczey et al., 2017). Patients on trial for CD19 chimeric antigen receptor (CAR)-T cells who receive Cy/Flu pre-conditioning had greater CAR-T expansion, persistence, and higher response rates than patients pre-conditioned with Cy alone (Turtle et al., 2016b). Cy/Flu pre-conditioning has been shown to increase efficacy through the enhanced engraftment and expansion of transferred T cells (Turtle et al., 2016b). The suggested mechanism of action of this pre-conditioning is to deplete

Figure 5. IL12-GEMy treatment induces T and NK cell activation

- (A) Naive or activated splenocytes from OT-I or OT-II mice were co-cultured with non-transduced control myeloid cells or IL12-GEMys at various ratios and IFN- γ was quantified by ELISA at 24 h. Statistical analysis was performed by unpaired t test at each ratio.
- (B) The expression of key T cell phenotype genes in bulk RNA isolated from the lungs of naive, tumor-bearing mice, or 8×10^6 IL12-GEMy treated tumor-bearing mice on day 15 post-primary tumor inoculation and 3 days after IL12-GEMy treatment ($n = 4$).
- (C) Violin plots of scRNA-seq data showing gene expression by cluster ($n = 4$). Statistical differences between groups analyzed by the Wilcoxon test. cyto T, cytotoxic T cells; non-cyto T, non-cytotoxic T cells; NK cells, natural killer cells; other Ly, other lymphocytes.
- (D) Ingenuity pathway analysis of cytotoxic T cell and NK cell clusters from single-cell RNA sequencing. Red bars indicate positive Z scores and blue bars indicate negative Z scores.
- (E) Cytotoxic T cell, non-cytotoxic T cell, NK cell, and other lymphocyte clusters were subsetted from the whole-lung scRNA-seq analysis and reclustered to identify more specific cell subsets. UMAP plots and the number of cells per cluster is shown. Statistical analysis between groups was performed by the Kolmogorov-Smirnov test of each cluster.
- (F) The expression level of genes associated with effector function and cytotoxicity in the high-resolution T and NK cell clusters. Statistical differences between groups analyzed by the Wilcoxon test.
- (G) M3-9-M ffluc-mCherry tumor-bearing mice were treated with 200 μ g of isotype, anti-CD8, or anti-CD4 antibody or 100 μ g of anti-NK1.1 antibody i.p. on days 9, 11, and 12 to induce depletion of cell populations. 8×10^6 IL12-GEMys were injected intravenously on day 12. Depletion antibody treatment was continued at 200 μ g per dose every 3–5 days for the duration of the experiment. Survival and tumor growth of mice treated with IL12-GEMys and antibody depletion regimens are shown ($n = 9$). Survival data were tested for significance by a log-rank (Mantel-Cox) test. **** $p < 0.0001$; *** $0.0001 < p < 0.001$; ** $0.001 < p < 0.01$; * $0.01 < p < 0.05$. In line graphs, data are represented as mean \pm SEM. In boxplots, the center line represents the median, the box limits denote the 25th to the 75th percentile, and the whiskers represent the minimum and maximum value. See also Figure S6H and Figure S7A.

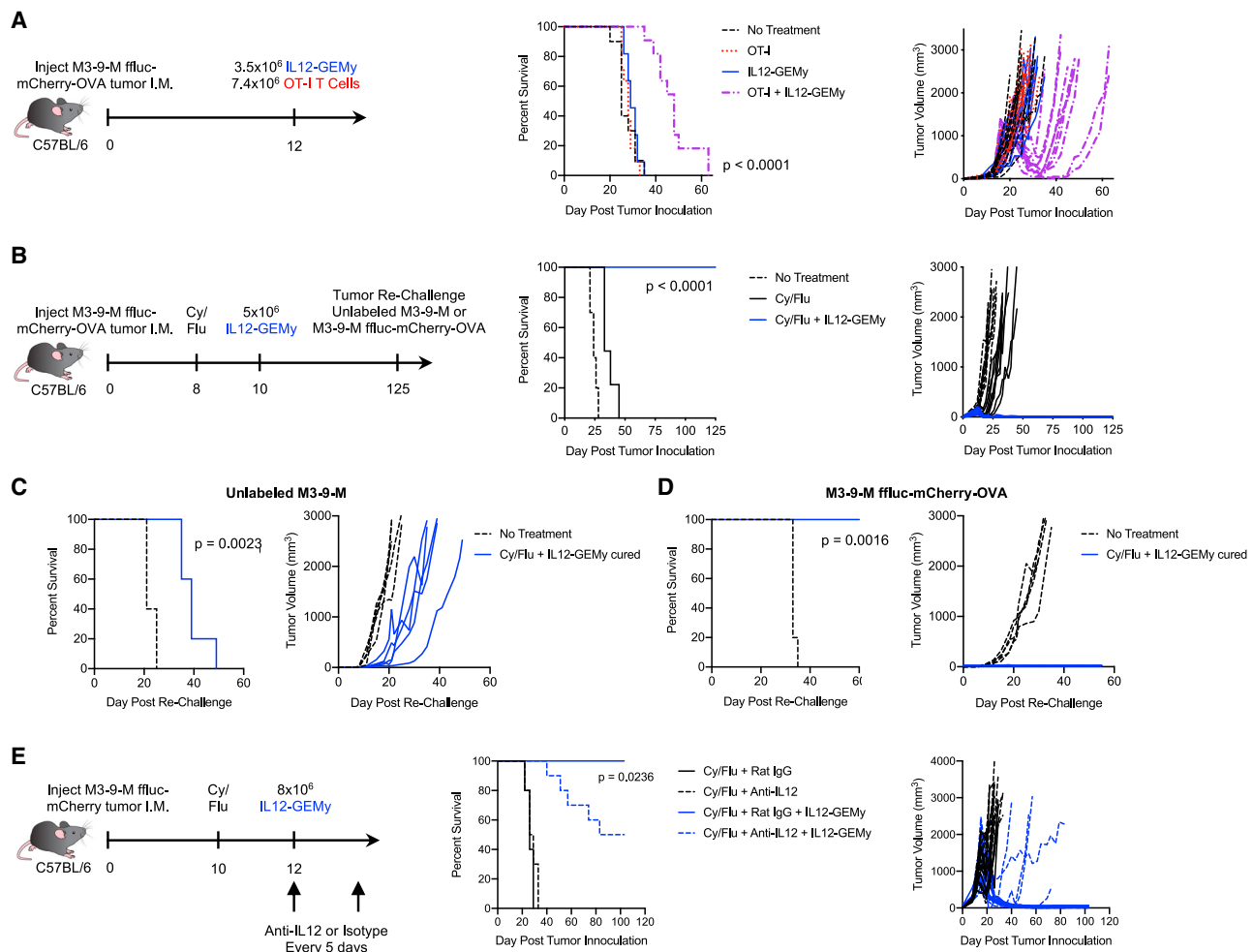


Figure 6. IL12-GEMy treatment is enhanced by combination with adoptive transfer of tumor-specific CD8⁺ T cells or chemotherapy pre-conditioning and generates long-lived tumor-specific memory

(A) Mice were orthotopically injected with M3-9-M ffluc-mCherry-OVA tumors. Mice received either no treatment (n = 10), 7.4 × 10⁶ OT-I T cells (n = 11), 3.5 × 10⁶ IL12-GEMy (n = 11), or both (n = 11) intravenously on day 12.

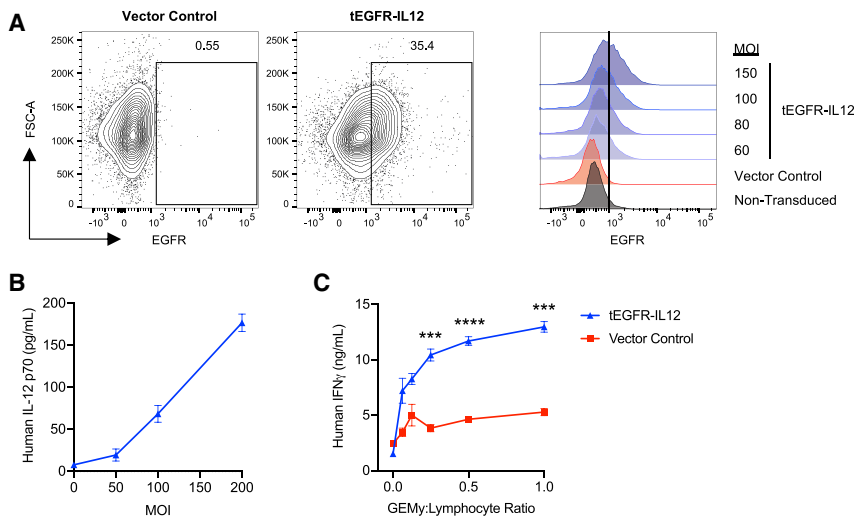
(B) Mice were orthotopically injected with M3-9-M ffluc-mCherry-OVA and treated with 2 mg of cyclophosphamide and 5 mg of fludarabine i.p. on day 8. Mice received 5 × 10⁶ IL12-GEMys intravenously on day 10. Survival and tumor growth were monitored over time (no treatment n = 10, Cy/Flu n = 9, Cy/Flu + IL12-GEMy n = 10).

(C) and (D) IL12-GEMy-cured mice were re-challenged with (C) unlabeled M3-9-M cells or (D) M3-9-M ffluc-mCherry-OVA in the contralateral leg compared to naive age-matched controls (n = 5).

(E) Mice were orthotopically injected with M3-9-M ffluc-mCherry tumor, treated with 2 mg of cyclophosphamide and 5 mg of fludarabine i.p. on day 10, and 8 × 10⁶ IL12-GEMys on day 12. Anti-IL12 or Rat IgG isotype antibody was administered starting on day 12 and every 5 days for the duration of the experiment (n = 10). Survival data were tested for significance by log-rank (Mantel-Cox) test. See also Figure S7.

endogenous peripheral immune cells to create immunological space and increase the availability of cytokines for the homeostatic expansion of transferred cells (Bracci et al., 2007; Hirayama et al., 2019; Neelapu, 2019). We observed lower levels of circulating T cells following Cy/Flu pre-conditioning, while myeloid populations were not impacted (Figure S7D). Lymphodepletion is a transient phenomenon, with endogenous lymphocyte populations rebounding by homeostatic proliferation (Sistigu et al., 2011). Notably, when combined with a single-dose pre-conditioning regimen of Cy/Flu 2 days preceding cell transfer, IL12-GEMy cell therapy resulted in durable cures (>100 days)

of mice with established primary tumors (Figure 6B). Cy/Flu pre-conditioning significantly increased the presence of transduced IL12-GEMy cells in the lungs but not primary tumors of mice 4 days after injection (Figure S7E). The presence of IL12-GEMys in the lung decreases over time, indicating that the cell product does not have long-term persistence *in vivo* (Figure S7E). We observe an increased trend in IL-12 levels and a 10-fold increase in IFN-γ levels in the lungs and primary tumors of mice treated with Cy/Flu and IL12-GEMys compared to IL12-GEMys without Cy/Flu pre-conditioning (Figure S7F). This enhanced IFN-γ response is associated with a robust expansion of PD-1⁺Lag3⁺

**Figure 7. Generation of human IL12-GEMys**

Human monocyte SC cells were transduced with vector control or tEGFR-IL12 lentiviral vector for 24 h.

(A) Transduction efficiency was measured by flow cytometry staining of truncated epidermal growth factor receptor (tEGFR) expression with varying multiplicity of infection (MOI) at 24 h. Representative flow plots of MOI 150 are shown.

(B) IL12-GEMys were washed after 24 h transduction and cultured for an additional 3 days. Human IL-12 production was measured by ELISA.

(C) Vector-control or tEGFR-IL12 monocyte SC cells were transduced at an MOI of 150 for 24 h, washed, and co-cultured with donor lymphocytes stimulated with TransAct beads and 40 units/mL of recombinant human IL-2 at varying GEMy:Lymphocyte ratios. Supernatant was collected at 24 h and analyzed for IFN- γ production by ELISA.

Statistical analysis was performed by unpaired t tests for each ratio. ***p < 0.0001; **0.001 < p < 0.001; **0.001 < p < 0.01; *0.01 < p < 0.05. Data are represented as mean ± SEM.

CD8 $^{+}$ T cells in both the lung and tumor, with the response peaking earlier in the lung at 1 week after treatment and later in the primary tumor, close to 20 days after IL12-GEMy injection (Figure S7G). We observe a contraction of this CD8 $^{+}$ T cell response with resolution and cure of the tumors (Figure S7G). Together, these data demonstrate that a small, transient number of IL12-GEMys in the context of Cy/Flu pre-conditioning has the ability to induce a robust immune response in the pre-metastatic niche of the lung and in the primary tumor, resulting in tumor regression and long-term cure.

IL-12 can act on effector T cells to promote the production of memory T cells that persist in a functional immune response and provide protective immunity (Xiao et al., 2009). In order to interrogate IL12-GEMy function in eliciting a memory response, cured mice were re-challenged with either unlabeled tumor or the original OVA-expressing tumor in the contralateral leg. When re-challenged with unlabeled M3-9-M, lacking the strong OVA antigen, IL12-GEMy-cured mice displayed a statistically significant delay in tumor growth relative to age-matched naive controls ($p = 0.0023$), evidence that IL12-GEMys elicit endogenous T cell responses that recognize multiple tumor antigens, including non-dominant antigens (Figure 6C). Cured mice re-challenged over 100 days post-IL12-GEMy treatment with the original tumor line were immune and did not develop tumors, consistent with the generation of functional memory T cells (Figure 6D).

We investigated the role of IL-12 in the maintenance of IL12-GEMy-induced remission. Mice were treated with anti-IL12 or isotype antibody and IL-12 depletion in the serum was confirmed by ELISA (Figure S7H). 50% of mice receiving anti-IL12 blocking antibody relapsed, suggesting that IL-12 is required for long-term tumor control (Figure 6E).

Together, these studies demonstrate that IL12-GEMys support the function of tumor-specific CD8 $^{+}$ T cells by enhancing suboptimal T cell therapy and that IL12-GEMy therapy in combination with Cy/Flu pre-conditioning is capable of generating durable cures with endogenous T cell memory to multiple antigens. This stimulation of adaptive immune responses coupled with the

reversal of the immune suppression program has a profound impact on tumor and metastatic progression.

Generation of human IL12-GEMys

To translate our findings into the human setting, we transduced human monocyte SC cells with lentiviral vector encoding human IL-12 with truncated epidermal growth factor receptor (tEGFR) as a reporter for transduction efficiency (Figures 7A and 7B). To test the ability of human IL12-GEMys to induce IFN- γ production by T cells, human IL12-GEMys were co-cultured with bead-stimulated donor human lymphocytes at varying ratios. Human IL12-GEMys significantly increased the secretion of IFN- γ by human lymphocytes compared to vector-control-transduced SC cells (Figure 7C). These data demonstrate the expression of functional IL-12 in a human monocyte cell line and their ability to induce IFN- γ production by human lymphocytes.

DISCUSSION

We found that there is a marked myeloid-derived core immune suppression transcriptional signature in the pre-metastatic lung. We demonstrate that this pre-metastatic niche signature is a coordinated, multigenic program that induces the upregulation of many genes, while few genes are downregulated (Figure 1C), signifying an active immune suppression process rather than a failure of adaptive immune activation. Further, we identified parallels in myeloid-mediated immune suppression genes between the pre-metastatic niche and the human bone-marrow stem cell niche (Figure S4). Although this transcriptional signature is most notably upregulated in myeloid cell populations, it is important to acknowledge that multiple other cell types also contribute to this immunosuppressive program and others features of the pre-metastatic niche (Murgai et al., 2017; Liu and Cao, 2016). These findings are remarkably consistent with transcriptomic profiling of pre/early metastatic microenvironment by other groups with diverse metastatic tumor models (Figure S2D) (Hiratsuka et al., 2008; Liu et al., 2016; Shao et al., 2018;

Yamamoto et al., 2008; Lee et al., 2019). Our study provides a better understanding of how various cell types in the pre-metastatic niche create an immunoregulatory environment.

The application of myeloid cells as a platform to reshape immunosuppressive microenvironments is a previously unappreciated strategy to target cancer progression. There is a large body of literature highlighting the importance of myeloid cell homing to human tumors and metastatic sites (Gabrilovich, 2017; Gabrilovich et al., 2012; Kumar et al., 2016; Qian et al., 2009; Veglia et al., 2019; Albrengues et al., 2018; Guldner et al., 2020). In our pre-clinical models, the introduction of IL12-GEMys reversed the core immune suppression gene program (Figure 3B) by disrupting the pre-metastatic niche environment to establish effective adaptive immunity (Figures 5B–5F), demonstrating the powerful impact that myeloid cells have in orchestrating immune responses. We highlight that the adoptive transfer of IL12-GEMys drives the plasticity of multiple different cell types toward an antitumor phenotype (Figures 3E–3G), suggesting that reversing these immunosuppressive programs in lieu of depleting specific cell populations is an effective therapeutic strategy. Although myeloid cell depletion is an active area of investigation that holds promise, this approach is not without shortcomings (Awad et al., 2018). The depletion of immunostimulatory myeloid populations can enhance tumor growth, myeloablative therapy leaves patients immunocompromised and at risk for life-threatening infections, and myeloid depletion may result in a rebound of immunosuppressive myeloid populations produced by the bone marrow that can accelerate tumor progression (Awad et al., 2018; Bonapace et al., 2014). Furthermore, despite multiple studies implicating any one particular cell population, our data highlight that a single cell type is not responsible for immune suppression; rather, immune suppression is driven by a transcriptional program expressed in many interacting cell populations. Given the diversity of myeloid populations, the individual contribution of specific cell types and differentiation states within the IL12-GEMy product is still not fully characterized; however, we hypothesize that the heterogeneity of the cell product is an advantageous quality as different cell types can possess varying levels of persistence, homing, and functionality that come together for remarkable therapeutic efficacy. We show that, despite the findings that IL12-GEMys have a low transduction efficiency (Figure S5A), have limited persistence (Figure S7E), and induce transiently elevated IL-12 and IFN- γ levels *in vivo* (Figure 2D; Figure S5C), we observe long-lasting tumor control (Figures 4 and 6). Our data with IL-12 inhibition suggest that immune surveillance is IL-12 dependent (Figure 6E). Particularly in the context of Cy/Flu, we observe significantly higher induction of IFN- γ responses in the lung and primary tumor by IL12-GEMys (Figure S7F) that is associated with increased CD8 $^{+}$ T cell responses (Figure S7G) and complete tumor regression (Figure 6B). We postulate that durable cures induced by IL12-GEMy treatment may result from the generation of functional memory T cells to anti-tumor targets (Figures 6B–6D) without the need for the long-term persistence of the IL12-GEMys themselves. However, there may be a small population of long-lived cells in the IL12-GEMy product that persists and maintains immune surveillance. These questions are areas of future investigation.

Many current immunotherapeutic strategies are based on mounting T cell responses to specific tumor antigens. The advantage of the myeloid-based approach is the *in vivo* activation of endogenous T cells and NK cells to mount a more complete immune response paired with the downregulation of immune suppression that often limits the efficacy of T cell-based approaches. Our findings from scRNA-seq of lymphocyte subpopulations demonstrate selective and coordinated cell-type-specific responses to IL-12 that result in effective anti-tumor immunity and may be exploited for future combination approaches with IL12-GEMys (Figure 5). Further, the observation that IL12-GEMys can impact cancer progression in the context of both lung and liver metastatic models highlights the potential application to multiple solid tumor malignancies (Figure 4). With elevated lung cytokine levels in the lung metastatic sarcoma model (Figure S5C), we predict that the homing of GEMys is linked to site-specific metastasis. The ability of GEMys to deliver cargo to metastatic sites other than the lung in tumor models that metastasize to other tissues is an area of great therapeutic potential. This technology could provide a platform to capitalize on the intrinsic specificity of myeloid cell homing to the earliest sites of metastases when the lesions might be most susceptible to reversal of immune suppression and activation of T cell immunity. Our studies also suggest that myeloid cells could be successfully combined with T cell-based immunotherapies (Figure 6A), providing rationale for future combination to enhance CAR-T cell and transgenic T cell receptor approaches for the treatment of solid tumors, which are limited by myeloid-mediated immune suppression (Li et al., 2019; Long et al., 2016; Rodriguez-Garcia et al., 2020). We also demonstrate that Cy/Flu chemotherapy pre-conditioning enhances IL12-GEMy efficacy, resulting in tumor regression and durable cures in our pre-clinical metastatic models (Figures 6B–6D). Further investigations into the mechanism of chemotherapy-mediated improvement of IL12-GEMy therapy are needed.

Together with our preliminary studies in human IL12-GEMys (Figure 7), our data provide a rationale for the clinical application of IL12-GEMys for the treatment of various late-stage malignancies. This body of work opens up exciting avenues for translation, with active investigations into human monocyte persistence, fate decisions of myeloid progenitor cells, and selection of the optimal starting population for the human IL12-GEMy cell product for clinical development. Truncated EGFR is included in the human construct for the monitoring of transduction efficiency, tracking of cells, and for safety to allow cell depletion with cetuximab (anti-EGFR) administration. GEMys can be configured to express variable cargos, receptors, and safety switches, with inducible tissue-specific expression for fine-tuned modulation of the microenvironment. Our vision for this platform in patients with high-risk solid tumors is to have cells collected up front for GEMy production and given to locally activate an immune response and limit the immune evasion responsible for break in tumor dormancy and metastatic outgrowth. This approach has the potential to promote long-lived anti-tumor T cells needed for durable remissions. Our work and others' support the development of myeloid cell-based therapy as a disruptive technology in the field of immunotherapy (Klichinsky et al., 2020; Bremelis et al., 2020; Gardell et al., 2020). More broadly,

this platform holds promise for harnessing cell-cell communication in both immune and non-immune cell populations to rebalance dysregulated niches in many diseases. Repurposing of targeted agents that demonstrate limited benefit when administered systemically provide a wealth of opportunities for future GEMy cargo. GEMys can also be designed to deliver factors to target other non-immune mechanisms mediating pre-metastatic niche formation and metastatic progression.

Together, our data provide valuable insight into the cell populations that contribute to a core transcriptional signature of immune suppression in the pre-metastatic niche. Our investigations suggest that the introduction of IL12-GEMys into the local milieu can result in profound transcriptional reprogramming in the pre-metastatic niche environment to subvert immune evasion by disseminated tumor cells. Ultimately, we demonstrate that perturbation of this immunosuppressive microenvironment with the innovative IL12-GEMy immunotherapy platform can have a profound impact on the progression of tumor growth and metastasis. The ability of myeloid cells to locally deliver cytokines or other biological mediators suggests that the applicability of such a platform could extend beyond the immune axis to deliver other key niche modulatory signals with potential application to diseases other than cancer.

Limitations of study

This study demonstrates a proof of concept for genetically engineering myeloid cells for the treatment of cancer. Additional work will be necessary to translate and evaluate the efficacy of this approach as a human therapy. First, in these studies the mouse bone-marrow-derived GEMy cell product is a heterogeneous population of cells. The contributions and persistence of specific cell types has not yet been elucidated. Further, these studies were performed in mouse models that may be more susceptible to immunologic targeting than human tumors and cytokine toxicity may be different in animal models compared to humans. Therefore, the safety switch design in the human studies will be important to limit potential toxicity. Acknowledging these limitations, we can see tantalizing future possibilities based on the findings from this cell-therapy platform to reprogram the dysregulated microenvironment.

STAR★METHODS

Detailed methods are provided in the online version of this paper and include the following:

- KEY RESOURCES TABLE
- RESOURCE AVAILABILITY
 - Lead contact
 - Materials availability
 - Data and code availability
- EXPERIMENTAL MODEL AND SUBJECT DETAILS
 - Mice
 - Cell lines
- METHOD DETAILS
 - Tumor models
 - Bioluminescent tumor cell tracking
 - Lentivirus production

- Murine IL12-GEMy production
- Tissue processing
- Flow cytometry
- Cytokine Analysis
- Chemotherapy treatment
- Antibody treatment
- T cell co-culture experiments
- T cell activation for adoptive transfer
- Immunofluorescence
- Bulk RNA sequencing
- Gene set enrichment analysis
- Pre-metastatic niche gene signature
- Single-cell RNA sequencing
- Comparison of IL12-GEMy bulk data with scRNA-seq data
- Human IL12-GEMy product
- Human IL12-GEMy co-culture with lymphocytes
- Statistical analysis

ACKNOWLEDGMENTS

We thank Carol Thiele and Naomi Taylor for reviewing the manuscript. We thank Steven Highfill, Lucas Horn, and Claudia Palena for providing reagents and expertise. We thank Katherine McKinnon for expertise in antibody panel design and Sophia Brown for flow cytometry technical support. We thank Arnulfo Mendoza, John Buckley, Yun Chen, and Devorah Gallardo for technical support with animal procedures. We thank Gail McMullen, Mia Allin, Geneti Gaga, April Huang, and Elena Kuznetsova for assistance with animal studies. We thank Valerie Nguyen for assistance with data collection. We thank Haiyan Lei for support analyzing bulk RNA-seq data. We thank Erina He for illustrations. This work was supported by the US National Institutes of Health grants ZIA BC 011332 and ZIA BC 011334 to R.N.K. S.K. is an NCI Transition to Industry Fellow supported by the Intramural Research Program of the Center for Cancer Research, National Cancer Institute, National Institutes of Health, USA.

AUTHOR CONTRIBUTIONS

Conceptualization, R.N.K., S.K., and D.W.B.; methodology, S.K., D.W.B., M.M., J.D., H.Q., M.E.C., and M.C.K.; software, M.C.K., Z.R., V.G., and M.M.; validation, S.K., D.W.B., A.K.T., and J.D.; formal analysis, S.K., D.W.B., V.G., M.E.C., and M.C.K.; investigation, S.K., D.W.B., A.K.T., M.E.C., C.N., K.A.A., J.D., W.J., J.K., C.F.C., K.M.W., S.P., and Z.R.; data curation, M.C.K., Z.R., and V.G.; writing – original draft, R.N.K., S.K., and D.W.B.; writing – review & editing, R.N.K., S.K., D.W.B., A.K.T., H.Q., V.G., and M.C.K.; visualization, S.K., D.W.B., A.K.T., V.G., and M.C.K.; supervision, R.N.K., S.H., and M.C.K.; project administration, R.N.K.; funding acquisition, R.N.K.

DECLARATION OF INTERESTS

S.K., D.W.B., H.Q., and R.N.K. are inventors on international patent application no. PCT/US2020/17515, “Genetically modified hematopoietic stem and progenitor cells (HSPCs) and mesenchymal cells as a platform to reduce or prevent metastasis, treat autoimmune and inflammatory disorders, and rebalance the immune milieu and dysregulated niches.” The remaining authors have no competing interests.

INCLUSION AND DIVERSITY

One or more of the authors of this paper self-identifies as an underrepresented ethnic minority in science. One or more of the authors of this paper received support from a program designed to increase minority representation in science. One or more of the authors of this paper self-identifies as living with a disability. One or more of the authors of this paper self-identifies as a member of the LGBTQ+ community.

Received: October 14, 2019

Revised: September 8, 2020

Accepted: February 22, 2021

Published: March 24, 2021

REFERENCES

- Albrengues, J., Shields, M.A., Ng, D., Park, C.G., Ambroico, A., Poindexter, M.E., Upadhyay, P., Uyeminami, D.L., Pommier, A., Küttner, V., et al. (2018). Neutrophil extracellular traps produced during inflammation awaken dormant cancer cells in mice. *Science* 361, eaao4227.
- Awad, R.M., De Vlaeminck, Y., Maebe, J., Goyaerts, C., and Breckpot, K. (2018). Turn Back the TIme: Targeting Tumor Infiltrating Myeloid Cells to Revert Cancer Progression. *Front. Immunol.* 9, 1977.
- Beury, D.W., Carter, K.A., Nelson, C., Sinha, P., Hanson, E., Nyandjo, M., Fitzgerald, P.J., Majeed, A., Wali, N., and Ostrand-Rosenberg, S. (2016). Myeloid-Derived Suppressor Cell Survival and Function Are Regulated by the Transcription Factor Nrf2. *J. Immunol.* 196, 3470–3478.
- Bonapace, L., Coissieux, M.M., Wyckoff, J., Mertz, K.D., Varga, Z., Junt, T., and Bentires-Alj, M. (2014). Cessation of CCL2 inhibition accelerates breast cancer metastasis by promoting angiogenesis. *Nature* 515, 130–133.
- Bracci, L., Moschella, F., Sestili, P., La Sorsa, V., Valentini, M., Canini, I., Baccarini, S., Maccari, S., Ramoni, C., Belardelli, F., and Proietti, E. (2007). Cyclophosphamide enhances the antitumor efficacy of adoptively transferred immune cells through the induction of cytokine expression, B-cell and T-cell homeostatic proliferation, and specific tumor infiltration. *Clin Cancer Res* 13, 644–653.
- Brembelis, K.J., Cowan, C.M., Kreuser, S.A., Labadie, K.P., Prieskorn, B.M., Lieberman, N.A.P., Ene, C.I., Moyes, K.W., Chinn, H., DeGolier, K.R., et al. (2020). Genetically engineered macrophages persist in solid tumors and locally deliver therapeutic proteins to activate immune responses. *J. Immunother. Cancer* 8. Published online September 30, 2020. <https://doi.org/10.1136/jitc-2020-001356>.
- Brunda, M.J., Luistro, L., Warrier, R.R., Wright, R.B., Hubbard, B.R., Murphy, M., Wolf, S.F., and Gately, M.K. (1993). Antitumor and antimetastatic activity of interleukin 12 against murine tumors. *J. Exp. Med.* 178, 1223–1230.
- Butler, A., Hoffman, P., Smibert, P., Papalexi, E., and Satija, R. (2018). Integrating single-cell transcriptomic data across different conditions, technologies, and species. *Nat. Biotechnol.* 36, 411–420.
- Cao, X., and Xu, J. (2019). Insights into inflammasome and its research advances in cancer. *Tumori* 105, 456–464.
- Casanova-Acebes, M., A-González, N., Weiss, L.A., and Hidalgo, A. (2014). Innate immune cells as homeostatic regulators of the hematopoietic niche. *Int. J. Hematol.* 99, 685–694.
- Chen, J., López-Moyado, I.F., Seo, H., Lio, C.J., Hempleman, L.J., Sekiya, T., Yoshimura, A., Scott-Browne, J.P., and Rao, A. (2019). NR4A transcription factors limit CAR T cell function in solid tumours. *Nature* 567, 530–534.
- Christoph Hafemeister, R.S. (2019). Normalization and variance stabilization of single-cell RNA-seq data using regularized negative binomial regression. *Genome Biol.* 20, 296.
- Colombo, M.P., and Trinchieri, G. (2002). Interleukin-12 in anti-tumor immunity and immunotherapy. *Cytokine Growth Factor Rev.* 13, 155–168.
- Croasdell, A., Duffney, P.F., Kim, N., Lacy, S.H., Sime, P.J., and Phipps, R.P. (2015). PPAR γ and the Innate Immune System Mediate the Resolution of Inflammation. *PPAR Res.* 2015, 549691.
- Davidson, S.M., Jonas, O., Keibler, M.A., Hou, H.W., Luengo, A., Mayers, J.R., Wyckoff, J., Del Rosario, A.M., Whitman, M., Chin, C.R., et al. (2017). Direct evidence for cancer-cell-autonomous extracellular protein catabolism in pancreatic tumors. *Nat. Med.* 23, 235–241.
- Davis, S., and Meltzer, P.S. (2007). GEOquery: a bridge between the Gene Expression Omnibus (GEO) and BioConductor. *Bioinformatics* 23, 1846–1847.
- Del Vecchio, M., Bajetta, E., Canova, S., Lotze, M.T., Wesa, A., Parmiani, G., and Anichini, A. (2007). Interleukin-12: biological properties and clinical application. *Clin. Cancer Res.* 13, 4677–4685.
- Dull, T., Zufferey, R., Kelly, M., Mandel, R.J., Nguyen, M., Trono, D., and Naldini, L. (1998). A third-generation lentivirus vector with a conditional packaging system. *J. Virol.* 72, 8463–8471.
- Finak, G., McDavid, A., Yajima, M., Deng, J., Gersuk, V., Shalek, A.K., Slichter, C.K., Miller, H.W., McElrath, M.J., Prlic, M., et al. (2015). MAST: a flexible statistical framework for assessing transcriptional changes and characterizing heterogeneity in single-cell RNA sequencing data. *Genome Biol.* 16, 278.
- Fujimura, T., Kambayashi, Y., and Aiba, S. (2012). Crosstalk between regulatory T cells (Tregs) and myeloid derived suppressor cells (MDSCs) during melanoma growth. *Oncolmumonology* 1, 1433–1434.
- Gabrilovich, D.I. (2017). Myeloid-Derived Suppressor Cells. *Cancer Immunol. Res.* 5, 3–8.
- Gabrilovich, D.I., Ostrand-Rosenberg, S., and Bronte, V. (2012). Coordinated regulation of myeloid cells by tumours. *Nat. Rev. Immunol.* 12, 253–268.
- Gajewski, T.F., Meng, Y., and Harlin, H. (2006). Immune suppression in the tumor microenvironment. *J. Immunother.* 29, 233–240.
- Gardell, J.L., Matsumoto, L.R., Chinn, H., DeGolier, K.R., Kreuser, S.A., Prieskorn, B., Balcaitis, S., Davis, A., Ellenbogen, R.G., and Crane, C.A. (2020). Human macrophages engineered to secrete a bispecific T cell engager support antigen-dependent T cell responses to glioblastoma. *J. Immunother. Cancer* 8. Published online September 30, 2020. <https://doi.org/10.1136/jitc-2020-001202>.
- Gentleman, R.C., Carey, V.J., Bates, D.M., Bolstad, B., Detting, M., Dudoit, S., Ellis, B., Gautier, L., Ge, Y., Gentry, J., et al. (2004). Bioconductor: open software development for computational biology and bioinformatics. *Genome Biol.* 5, R80.
- Giles, A.J., Reid, C.M., Evans, J.D., Murgai, M., Vicioso, Y., Highfill, S.L., Kasai, M., Vahdat, L., Mackall, C.L., Lyden, D., et al. (2016). Activation of Hematopoietic Stem/Progenitor Cells Promotes Immunosuppression Within the Pre-metastatic Niche. *Cancer Res.* 76, 1335–1347.
- Grzywa, T.M., Sosnowska, A., Matryba, P., Rydzynska, Z., Jasinski, M., Nowis, D., and Golab, J. (2020). Myeloid Cell-Derived Arginase in Cancer Immune Response. *Front. Immunol.* 11, 938.
- Gui, J., Zahedi, F., Ortiz, A., Cho, C., Katlinski, K.V., Alicea-Torres, K., Li, J., Todd, L., Zhang, H., Beiting, D.P., et al. (2020). Activation of p38 α stress-activated protein kinase drives the formation of the pre-metastatic niche in the lungs. *Nat. Can.* 1, 603–619.
- Guldner, I.H., Wang, Q., Yang, L., Golomb, S.M., Zhao, Z., Lopez, J.A., Brunory, A., Howe, E.N., Zhang, Y., Palakurthi, B., et al. (2020). CNS-Native Myeloid Cells Drive Immune Suppression in the Brain Metastatic Niche through Cxcl10. *Cell* 183, 1234–1248.e25.
- Guo, B., Fu, S., Zhang, J., Liu, B., and Li, Z. (2016). Targeting inflammasome/IL-1 pathways for cancer immunotherapy. *Sci. Rep.* 6, 36107.
- Hadley, W. (2016). *Ggplot2* (Springer).
- Hay, S.B., Ferchen, K., Chetal, K., Grimes, H.L., and Salomonis, N. (2018). The Human Cell Atlas bone marrow single-cell interactive web portal. *Exp. Hematol.* 68, 51–61.
- Heczey, A., Louis, C.U., Savoldo, B., Dakhova, O., Durett, A., Grilley, B., Liu, H., Wu, M.F., Mei, Z., Gee, A., et al. (2017). CAR T Cells Administered in Combination with Lymphodepletion and PD-1 Inhibition to Patients with Neuroblastoma. *Mol. Ther.* 25, 2214–2224.
- Hiratsuka, S., Nakamura, K., Iwai, S., Murakami, M., Itoh, T., Kijima, H., Shipley, J.M., Senior, R.M., and Shibuya, M. (2002). MMP9 induction by vascular endothelial growth factor receptor-1 is involved in lung-specific metastasis. *Cancer Cell* 2, 289–300.
- Hiratsuka, S., Watanabe, A., Sakurai, Y., Akashi-Takamura, S., Ishibashi, S., Miyake, K., Shibuya, M., Akira, S., Aburatani, H., and Maru, Y. (2008). The S100A8-serum amyloid A3-TLR4 paracrine cascade establishes a pre-metastatic phase. *Nat. Cell Biol.* 10, 1349–1355.
- Hirayama, A.V., Gauthier, J., Hay, K.A., Voutsinas, J.M., Wu, Q., Gooley, T., Li, D., Cherian, S., Chen, X., Pender, B.S., et al. (2019). The response to lympho-depletion impacts PFS in patients with aggressive non-Hodgkin lymphoma treated with CD19 CAR T cells. *Blood* 133, 1876–1887.

- Hong, I.S. (2016). Stimulatory versus suppressive effects of GM-CSF on tumor progression in multiple cancer types. *Exp. Mol. Med.* 48, e242.
- Hong, C., Kidani, Y., A-Gonzalez, N., Phung, T., Ito, A., Rong, X., Ericson, K., Mikkola, H., Beaven, S.W., Miller, L.S., et al. (2012). Coordinate regulation of neutrophil homeostasis by liver X receptors in mice. *J. Clin. Invest.* 122, 337–347.
- Høye, A.M., and Erler, J.T. (2016). Structural ECM components in the pre-metastatic and metastatic niche. *Am. J. Physiol. Cell Physiol.* 310, C955–C967.
- Hutloff, A., Dittrich, A.M., Beier, K.C., Eljaschewitsch, B., Kraft, R., Anagnostopoulos, I., and Kroczeck, R.A. (1999). ICOS is an inducible T-cell co-stimulator structurally and functionally related to CD28. *Nature* 397, 263–266.
- Joyce, J.A., and Pollard, J.W. (2009). Microenvironmental regulation of metastasis. *Nat. Rev. Cancer* 9, 239–252.
- Kaczanowska, S., and Kaplan, R.N. (2020). Mapping the switch that drives the pre-metastatic niche. *Nat. Can.* 1, 577–579.
- Kaneda, M.M., Messer, K.S., Ralainirina, N., Li, H., Leem, C.J., Gorjestani, S., Woo, G., Nguyen, A.V., Figueiredo, C.C., Fouquet, P., et al. (2016). PI3K γ is a molecular switch that controls immune suppression. *Nature* 539, 437–442.
- Kaplan, R.N., Riba, R.D., Zacharoulis, S., Bramley, A.H., Vincent, L., Costa, C., MacDonald, D.D., Jin, D.K., Shido, K., Kerns, S.A., et al. (2005). VEGFR1-positive haematopoietic bone marrow progenitors initiate the pre-metastatic niche. *Nature* 438, 820–827.
- Katzenellenbogen, Y., Sheban, F., Yalin, A., Yofe, I., Svetlichny, D., Jaitin, D.A., Bernstein, C., Moshe, A., Keren-Shaul, H., Cohen, M., et al. (2020). Coupled scRNA-Seq and Intracellular Protein Activity Reveal an Immunosuppressive Role of TREM2 in Cancer. *Cell* 182, 872–885.
- Kerkar, S.P., Goldszmid, R.S., Muranski, P., Chinnasamy, D., Yu, Z., Reger, R.N., Leonardi, A.J., Morgan, R.A., Wang, E., Marincola, F.M., et al. (2011). IL-12 triggers a programmatic change in dysfunctional myeloid-derived cells within mouse tumors. *J. Clin. Invest.* 121, 4746–4757.
- Klichinsky, M., Ruella, M., Shestova, O., Lu, X.M., Best, A., Zeeman, M., Schmierer, M., Gabrusiewicz, K., Anderson, N.R., Petty, N.E., et al. (2020). Human chimeric antigen receptor macrophages for cancer immunotherapy. *Nat. Biotechnol.* 38, 947–953.
- Ko, J.H., Lee, H.J., Jeong, H.J., and Oh, J.Y. (2017). Ly6C hi monocytes are required for mesenchymal stem/stromal cell-induced immune tolerance in mice with experimental autoimmune uveitis. *Biochem. Biophys. Res. Commun.* 494, 6–12.
- Koeffler, H.P. (2003). Peroxisome proliferator-activated receptor gamma and cancers. *Clin. Cancer Res.* 9, 1–9.
- Korotkevich, G., Sukhov, V., and Sergushichev, A. (2019). Fast gene set enrichment analysis. *bioRxiv*, 060012.
- Kumar, V., Patel, S., Tcyganov, E., and Gabrilovich, D.I. (2016). The Nature of Myeloid-Derived Suppressor Cells in the Tumor Microenvironment. *Trends Immunol.* 37, 208–220.
- Lee, J.W., Komar, C.A., Bengsch, F., Graham, K., and Beatty, G.L. (2016). Genetically Engineered Mouse Models of Pancreatic Cancer: The KPC Model (LSL-Kras(G12D/+); LSL-Trp53(R172H/+); Pdx-1-Cre), Its Variants, and Their Application in Immuno-oncology Drug Discovery. *Curr. Protoc. Pharmacol.* 73, 14.39.1–14.39.20.
- Lee, J.W., Stone, M.L., Porrett, P.M., Thomas, S.K., Komar, C.A., Li, J.H., Delman, D., Graham, K., Gladney, W.L., Hua, X., et al. (2019). Hepatocytes direct the formation of a pro-metastatic niche in the liver. *Nature* 567, 249–252.
- Li, D., Li, X., Zhou, W.L., Huang, Y., Liang, X., Jiang, L., Yang, X., Sun, J., Li, Z., Han, W.D., and Wang, W. (2019). Genetically engineered T cells for cancer immunotherapy. *Signal Transduct. Target. Ther.* 4, 35.
- Liu, Y., and Cao, X. (2016). Characteristics and Significance of the Pre-metastatic Niche. *Cancer Cell* 30, 668–681.
- Liu, Y., Gu, Y., Han, Y., Zhang, Q., Jiang, Z., Zhang, X., Huang, B., Xu, X., Zheng, J., and Cao, X. (2016). Tumor Exosomal RNAs Promote Lung Pre-metastatic Niche Formation by Activating Alveolar Epithelial TLR3 to Recruit Neutrophils. *Cancer Cell* 30, 243–256.
- Long, A.H., Highfill, S.L., Cui, Y., Smith, J.P., Walker, A.J., Ramakrishna, S., El-Etriby, R., Galli, S., Tsokos, M.G., Orentas, R.J., and Mackall, C.L. (2016). Reduction of MDSCs with All-trans Retinoic Acid Improves CAR Therapy Efficacy for Sarcomas. *Cancer Immunol. Res.* 4, 869–880.
- Mantovani, A., Barajon, I., and Garlanda, C. (2018). IL-1 and IL-1 regulatory pathways in cancer progression and therapy. *Immunol. Rev.* 281, 57–61.
- Martner, A., Aydin, E., and Hellstrand, K. (2019). NOX2 in autoimmunity, tumor growth and metastasis. *J. Pathol.* 247, 151–154.
- Maude, S.L., Barrett, D., Teachey, D.T., and Grupp, S.A. (2014). Managing cytokine release syndrome associated with novel T cell-engaging therapies. *Cancer J.* 20, 119–122.
- Meadors, J.L., Cui, Y., Chen, Q.R., Song, Y.K., Khan, J., Merlini, G., Tsokos, M., Orentas, R.J., and Mackall, C.L. (2011). Murine rhabdomyosarcoma is immunogenic and responsive to T-cell-based immunotherapy. *Pediatr. Blood Cancer* 57, 921–929.
- Morikawa, K., Walker, S.M., Nakajima, M., Pathak, S., Jessup, J.M., and Fidler, I.J. (1988). Influence of organ environment on the growth, selection, and metastasis of human colon carcinoma cells in nude mice. *Cancer Res.* 48, 6863–6871.
- Moyes, K.W., Lieberman, N.A., Kreuser, S.A., Chinn, H., Winter, C., Deutsch, G., Hoglund, V., Watson, R., and Crane, C.A. (2017). Genetically Engineered Macrophages: A Potential Platform for Cancer Immunotherapy. *Hum. Gene Ther.* 28, 200–215.
- Murgai, M., Ju, W., Eason, M., Kline, J., Beury, D.W., Kaczanowska, S., Miettinen, M.M., Kruhlak, M., Lei, H., Shern, J.F., et al. (2017). KLF4-dependent perivascular cell plasticity mediates pre-metastatic niche formation and metastasis. *Nat. Med.* 23, 1176–1190.
- Mussar, K., Pardike, S., Hohl, T.M., Hardiman, G., Cirulli, V., and Crisa, L. (2017). A CCR2+ myeloid cell niche required for pancreatic β cell growth. *JCI Insight* 2, e93834.
- Nagaraj, S., Gupta, K., Pisarev, V., Kinarsky, L., Sherman, S., Kang, L., Herber, D.L., Schneck, J., and Gabrilovich, D.I. (2007). Altered recognition of antigen as a mechanism of CD8+ T cell tolerance in cancer. *Nat. Med.* 13, 828–835.
- Naik, S., Larsen, S.B., Cowley, C.J., and Fuchs, E. (2018). Two to Tango: Dialog between Immunity and Stem Cells in Health and Disease. *Cell* 175, 908–920.
- Neelapu, S.S. (2019). CAR-T efficacy: is conditioning the key? *Blood* 133, 1799–1800.
- Noelia, A.-G., and Castrillo, A. (2011). Liver X receptors as regulators of macrophage inflammatory and metabolic pathways. *Biochim. Biophys. Acta* 1812, 982–994.
- Obstfeld, A.E., Frey, N.V., Mansfield, K., Lacey, S.F., June, C.H., Porter, D.L., Melenhorst, J.J., and Wasik, M.A. (2017). Cytokine release syndrome associated with chimeric-antigen receptor T-cell therapy: clinicopathological insights. *Blood* 130, 2569–2572.
- Paget, S. (1899). The distribution of secondary growths in cancer of the breast. *Cancer Metastasis Rev.* 8, 98–101.
- Pappo, A.S., Anderson, J.R., Crist, W.M., Wharam, M.D., Breitfeld, P.P., Hawkins, D., Raney, R.B., Womer, R.B., Parham, D.M., Qualman, S.J., and Grier, H.E. (1999). Survival after relapse in children and adolescents with rhabdomyosarcoma: A report from the Intergroup Rhabdomyosarcoma Study Group. *J. Clin. Oncol.* 17, 3487–3493.
- Park, M.J., Lee, S.H., Kim, E.K., Lee, E.J., Baek, J.A., Park, S.H., Kwok, S.K., and Cho, M.L. (2018). Interleukin-10 produced by myeloid-derived suppressor cells is critical for the induction of Tregs and attenuation of rheumatoid inflammation in mice. *Sci. Rep.* 8, 3753.
- Peinado, H., Alečković, M., Lavotshkin, S., Matei, I., Costa-Silva, B., Moreno-Bueno, G., Hergueta-Redondo, M., Williams, C., García-Santos, G., Ghajar, C., et al. (2012). Melanoma exosomes educate bone marrow progenitor cells toward a pro-metastatic phenotype through MET. *Nat. Med.* 18, 883–891.
- Peinado, H., Zhang, H., Matei, I.R., Costa-Silva, B., Hoshino, A., Rodrigues, G., Psaila, B., Kaplan, R.N., Bromberg, J.F., Kang, Y., et al. (2017). Pre-metastatic niches: organ-specific homes for metastases. *Nat. Rev. Cancer* 17, 302–317.

- Pollard, J.W. (2004). Tumour-educated macrophages promote tumour progression and metastasis. *Nat. Rev. Cancer* 4, 71–78.
- Psaila, B., and Lyden, D. (2009). The metastatic niche: adapting the foreign soil. *Nat. Rev. Cancer* 9, 285–293.
- Qian, B., Deng, Y., Im, J.H., Muschel, R.J., Zou, Y., Li, J., Lang, R.A., and Pollard, J.W. (2009). A distinct macrophage population mediates metastatic breast cancer cell extravasation, establishment and growth. *PLoS ONE* 4, e6562.
- Rahmani, W., Liu, Y., Rosin, N.L., Kline, A., Raharjo, E., Yoon, J., Stratton, J.A., Sinha, S., and Biernaskie, J. (2018). Macrophages Promote Wound-Induced Hair Follicle Regeneration in a CX₃CR1- and TGF- β 1-Dependent Manner. *J. Invest. Dermatol.* 138, 2111–2122.
- Rodriguez-Garcia, A., Palazon, A., Noguera-Ortega, E., Powell, D.J., Jr., and Guedan, S. (2020). CAR-T Cells Hit the Tumor Microenvironment: Strategies to Overcome Tumor Escape. *Front. Immunol.* 11, 1109.
- Rove, K.O., and Crawford, E.D. (2009). Metastatic cancer in solid tumors and clinical outcome: skeletal-related events. *Oncology* 23, 21–27.
- Schilbach, K., Welker, C., Krickeberg, N., Kaißer, C., Schleicher, S., and Hashimoto, H. (2020). In the Absence of a TCR Signal IL-2/IL-12/18-Stimulated $\gamma\delta$ T Cells Demonstrate Potent Anti-Tumoral Function Through Direct Killing and Senescence Induction in Cancer Cells. *Cancers* 12, 130.
- Scully, O.J., Bay, B.H., Yip, G., and Yu, Y. (2012). Breast cancer metastasis. *Cancer Genomics Proteomics* 9, 311–320.
- Sehgal, A., Donaldson, D.S., Pridans, C., Sauter, K.A., Hume, D.A., and Mabbott, N.A. (2018). The role of CSF1R-dependent macrophages in control of the intestinal stem-cell niche. *Nat. Commun.* 9, 1272.
- Shao, Y., Chen, T., Zheng, X., Yang, S., Xu, K., Chen, X., Xu, F., Wang, L., Shen, Y., Wang, T., et al. (2018). Colorectal cancer-derived small extracellular vesicles establish an inflammatory premetastatic niche in liver metastasis. *Carcinogenesis* 39, 1368–1379.
- Sistigu, A., Vaud, S., Chaput, N., Bracci, L., Proietti, E., and Zitvogel, L. (2011). Immunomodulatory effects of cyclophosphamide and implementations for vaccine design. *Semin Immunopathol* 33, 369–383.
- Soares, K.C., Foley, K., Olino, K., Leubner, A., Mayo, S.C., Jain, A., Jaffee, E., Schulick, R.D., Yoshimura, K., Edil, B., and Zheng, L. (2014). A preclinical murine model of hepatic metastases. *J. Vis. Exp.* Published online September 27, 2014. <https://doi.org/10.3791/51677>.
- Soldevilla, M.M., Villanueva, H., Meraviglia-Crivelli, D., Menon, A.P., Ruiz, M., Cebollero, J., Villalba, M., Moreno, B., Lozano, T., Llopiz, D., Pejrenaute, A., Sarobe, P., and Pastor, F. (2019). ICOS Costimulation at the Tumor Site in Combination with CTLA-4 Blockade Therapy Elicits Strong Tumor Immunity. *Mol. Ther.* 27, 1878–1891.
- Steding, C.E., Wu, S.T., Zhang, Y., Jeng, M.H., Elzey, B.D., and Kao, C. (2011). The role of interleukin-12 on modulating myeloid-derived suppressor cells, increasing overall survival and reducing metastasis. *Immunology* 133, 221–238.
- Strauss, J., Heery, C.R., Kim, J.W., Jochems, C., Donahue, R.N., Montgomery, A.S., McMahon, S., Lampert, E., Marté, J.L., Madan, R.A., et al. (2019). First-in-Human Phase I Trial of a Tumor-Targeted Cytokine (NHS-IL12) in Subjects with Metastatic Solid Tumors. *Clin. Cancer Res.* 25, 99–109.
- Stuart, T., Butler, A., Hoffman, P., Hafemeister, C., Papalexi, E., Mauck, W.M., 3rd, Hao, Y., Stoeckius, M., Smibert, P., and Satija, R. (2019). Comprehensive Integration of Single-Cell Data. *Cell* 177, 1888–1902.
- Svensson, E., Christiansen, C.F., Ulrichsen, S.P., Rørth, M.R., and Sørensen, H.T. (2017). Survival after bone metastasis by primary cancer type: a Danish population-based cohort study. *BMJ Open* 7, e016022.
- Tatsumi, T., Huang, J., Gooding, W.E., Gambotto, A., Robbins, P.D., Vujanovic, N.L., Alber, S.M., Watkins, S.C., Okada, H., and Storkus, W.J. (2003). Intratumoral delivery of dendritic cells engineered to secrete both interleukin (IL)-12 and IL-18 effectively treats local and distant disease in association with broadly reactive Tc1-type immunity. *Cancer Res.* 63, 6378–6386.
- Tavazoie, M.F., Pollack, I., Tanqueco, R., Ostendorf, B.N., Reis, B.S., Goncalves, F.C., Kurth, I., Andreu-Agullo, C., Derbyshire, M.L., Posada, J., et al. (2018). LXR/ApoE Activation Restricts Innate Immune Suppression in Cancer. *Cell* 172, 825–840.
- Teng, J.J., Zhang, J., Zhang, T.Y., Zhang, S., and Li, B.S. (2015). Prognostic value of peripheral blood lymphocyte-to-monocyte ratio in patients with solid tumors: a meta-analysis. *Oncotargets Ther.* 9, 37–47.
- Turtle, C.J., Hanafi, L.A., Berger, C., Gooley, T.A., Cherian, S., Hudecek, M., Sommermeyer, D., Melville, K., Pender, B., Budiarso, T.M., et al. (2016a). CD19 CAR-T cells of defined CD4+:CD8+ composition in adult B cell ALL patients. *J. Clin. Invest.* 126, 2123–2138.
- Turtle, C.J., Hanafi, L.A., Berger, C., Hudecek, M., Pender, B., Robinson, E., Hawkins, R., Chaney, C., Cherian, S., Chen, X., et al. (2016b). Immunotherapy of non-Hodgkin's lymphoma with a defined ratio of CD8+ and CD4+ CD19-specific chimeric antigen receptor-modified T cells. *Sci Transl Med* 8, 355ra116.
- Veglia, F., Tyurin, V.A., Blasi, M., De Leo, A., Kossenkov, A.V., Donthireddy, L., To, T.K.J., Schug, Z., Basu, S., Wang, F., et al. (2019). Fatty acid transport protein 2 reprograms neutrophils in cancer. *Nature* 569, 73–78.
- Wang, S., Yang, J., Qian, J., Wezeman, M., Kwak, L.W., and Yi, Q. (2006). Tumor evasion of the immune system: inhibiting p38 MAPK signaling restores the function of dendritic cells in multiple myeloma. *Blood* 107, 2432–2439.
- Wang, G., van Driel, B.J., Liao, G., O'Keefe, M.S., Halibozek, P.J., Flipse, J., Yigit, B., Azcutia, V., Luscinskas, F.W., Wang, N., and Terhorst, C. (2015). Migration of myeloid cells during inflammation is differentially regulated by the cell surface receptors Slamf1 and Slamf8. *PLoS ONE* 10, e0121968.
- Wang, E.C.E., Dai, Z., Ferrante, A.W., Drake, C.G., and Christiano, A.M. (2019a). A Subset of TREM2⁺ Dermal Macrophages Secretes Oncostatin M to Maintain Hair Follicle Stem Cell Quiescence and Inhibit Hair Growth. *Cell Stem Cell* 24, 654–669.
- Wang, K., Xu, T., Ruan, H., Xiao, H., Liu, J., Song, Z., Cao, Q., Bao, L., Liu, D., Wang, C., et al. (2019b). LXR α promotes cell metastasis by regulating the NLRP3 inflammasome in renal cell carcinoma. *Cell Death Dis.* 10, 159.
- Welch, D.R., and Hurst, D.R. (2019). Defining the Hallmarks of Metastasis. *Cancer Res.* 79, 3011–3027.
- Wiens, A.L., and Hattab, E.M. (2014). The pathological spectrum of solid CNS metastases in the pediatric population. *J. Neurosurg. Pediatr.* 14, 129–135.
- Wolf, S.F., Temple, P.A., Kobayashi, M., Young, D., Dicig, M., Lowe, L., Dzialo, R., Fitz, L., Ferenz, C., Hewick, R.M., et al. (1991). Cloning of cDNA for natural killer cell stimulatory factor, a heterodimeric cytokine with multiple biologic effects on T and natural killer cells. *J. Immunol.* 146, 3074–3081.
- Xia, A., Zhang, Y., Xu, J., Yin, T., and Lu, X.J. (2019). T Cell Dysfunction in Cancer Immunity and Immunotherapy. *Front Immunol* 10, 1719.
- Xiao, Z., Casey, K.A., Jameson, S.C., Curtsinger, J.M., and Mescher, M.F. (2009). Programming for CD8 T cell memory development requires IL-12 or type I IFN. *J. Immunol.* 182, 2786–2794.
- Yamamoto, M., Kikuchi, H., Ohta, M., Kawabata, T., Hiramatsu, Y., Kondo, K., Baba, M., Kamiya, K., Tanaka, T., Kitagawa, M., and Konno, H. (2008). TSU68 prevents liver metastasis of colon cancer xenografts by modulating the premetastatic niche. *Cancer Res.* 68, 9754–9762.
- Yang, Z., Zhang, X., Darrah, P.A., and Mosser, D.M. (2010). The regulation of Th1 responses by the p38 MAPK. *J. Immunol.* 185, 6205–6213.
- Zhang, L., Kerkar, S.P., Yu, Z., Zheng, Z., Yang, S., Restifo, N.P., Rosenberg, S.A., and Morgan, R.A. (2011). Improving adoptive T cell therapy by targeting and controlling IL-12 expression to the tumor environment. *Mol. Ther.* 19, 751–759.
- Zhang, L., Morgan, R.A., Beane, J.D., Zheng, Z., Dudley, M.E., Kassim, S.H., Nahvi, A.V., Ngo, L.T., Sherry, R.M., Phan, G.Q., et al. (2015). Tumor-infiltrating lymphocytes genetically engineered with an inducible gene encoding interleukin-12 for the immunotherapy of metastatic melanoma. *Clin. Cancer Res.* 21, 2278–2288.
- Zhang, S., Ma, X., Zhu, C., Liu, L., Wang, G., and Yuan, X. (2016). The Role of Myeloid-Derived Suppressor Cells in Patients with Solid Tumors: A Meta-Analysis. *PLoS ONE* 11, e0164514.

STAR★METHODS

KEY RESOURCES TABLE

REAGENT or RESOURCE	SOURCE	IDENTIFIER
Antibodies		
Rat anti-mouse CD45, clone 30-F11	BD Biosciences	Cat# 564225, RRID:AB_2716861
Mouse anti-mouse CD45.1, clone A20	Biolegend	Cat# 110718, RRID:AB_492862
Mouse anti-mouse CD45.2, clone 104	Biolegend	Cat# 109839, RRID:AB_2562604
Mouse anti-rat CD90/mouse CD90.1 (Thy-1.1), clone OX-7	Biolegend	Cat# 202526, RRID:AB_1595470
Rat anti-mouse CD3, clone 17A2	Biolegend	Cat# 100217, RRID:AB_1595597
Rat anti-mouse CD4, clone RM4-5	Biolegend	Cat# 100528, RRID:AB_312729
Rat anti-mouse CD8, clone 53-6.7	Biolegend	Cat# 100714, RRID:AB_312753
Rat anti-mouse/human CD44, clone IM7	Biolegend	Cat# 103047, RRID:AB_2562451
Rat anti-mouse PD-1, clone 29F.1A12	Biolegend	Cat# 135205, RRID:AB_1877232
Rat anti-mouse Lag-3, clone C9B7W	Biolegend	Cat# 125221, RRID:AB_2572080
Rat anti-mouse CD19, clone 6D5	Biolegend	Cat# 115528, RRID:AB_493735
Mouse anti-mouse NK1.1, clone PK136	Biolegend	Cat# 108745, RRID:AB_2563286
Rat anti-mouse CD16/CD32, clone 93	eBioscience	Cat# 14-0161-82, RRID:AB_467133
Rat anti-mouse CD11b, clone M1/70	eBioscience	Cat# 14-0112-81, RRID:AB_467107
Rat anti-mouse CD11b, clone M1/70	Biolegend	Cat# 101228, RRID:AB_893232
Armenian Hamster anti-mouse CD11c, clone HL3	Biolegend	Cat# 117339, RRID:AB_2562414
Rat anti-mouse F4/80, clone BM8	Biolegend	Cat# 123110, RRID:AB_893486
Rat anti-mouse Ly6G, clone 1A8	Biolegend	Cat# 127624, RRID:AB_10640819
Rat anti-mouse Ly6C, clone HK1.4	Biolegend	Cat# 128024, RRID:AB_10643270
Rat anti-mouse CD43, clone S11	Biolegend	Cat# 143208, RRID:AB_11149685
Mouse anti-mouse H-2K ^b bound to SIINFEKL, clone 25-D1.16	Biolegend	Cat# 141604, RRID:AB_10895905
Mouse anti-human EGFR (Research Grade Cetuximab Biosimilar), clone Hu1	R&D Systems	Cat# FAB9577P
Mouse anti-human CD45 antibody, clone HI30	Biolegend	Cat# 304028, RRID:AB_893338
Mouse anti-human CD14 antibody, clone HCD14	Biolegend	Cat# 325610, RRID:AB_830683
<i>InVivomAb</i> rat anti-mouse CD8a, clone 2.43	BioXCell	Cat# BE0061, RRID:AB_1125541
<i>InVivomAb</i> rat anti-mouse CD4, clone GK1.5	BioXCell	Cat# BE0003-1, RRID:AB_1107636
<i>InVivomAb</i> rat anti-mouse NK1.1, clone PK136	BioXCell	Cat# BE0036, RRID:AB_1107737
<i>InVivomAb</i> rat IgG2b isotype control, clone LTF-2	BioXCell	Cat# BE0090, RRID:AB_1107780
<i>InVivoMAb</i> anti-mouse IL-12 p75, clone R2-9A5	BioXCell	Cat# BE0233, RRID:AB_2687715
CD4 Monoclonal Antibody, clone 4SM95	Thermo Fisher Scientific	Cat# 14-9766-80, RRID:AB_2573007
CD8a Monoclonal Antibody, clone 4SM16	Thermo Fisher Scientific	Cat# 14-0195-82, RRID:AB_2637159
Chemicals, peptides, and recombinant proteins		
Recombinant Mouse SCF Protein	R&D Systems	Cat# 455-MC-500
Recombinant Mouse FLT-3 Ligand Protein	R&D Systems	Cat# 427-FL-MTO
Recombinant Mouse IL-6 Protein	R&D Systems	Cat# 406-ML-MTO
Protamine Sulfate	Fresenius Kabi	Cat# C22905
Cyclophosphamide monohydrate	Sigma Aldrich	Cat# C0768-1G
Fludarabine phosphate	Actavis Pharma, Inc.	Cat# NDC 45963-609-55
Fludarabine phosphate	Leucadia Pharmaceuticals	NDC 24201-237-01
OVA ₂₅₇₋₂₆₄ (SIINFEKL)	AnaSpec, Inc.	Cat# AS-60193-1

(Continued on next page)

Continued

REAGENT or RESOURCE	SOURCE	IDENTIFIER
OVA ₃₂₃₋₃₃₉	AnaSpec, Inc.	Cat# AS-27024
Recombinant Human IL-2 Protein Proleukin® (aldesleukin)	Clinigen Group PLC	N/A
Critical commercial assays		
EasySep Mouse Hematopoietic Cell Isolation Kit	StemCell Technologies	Cat# 19856
Mouse IL-12 p70 DuoSet ELISA	R&D Systems	Cat# DY419
Mouse IL-12 p70 Quantikine ELISA	R&D Systems	Cat# M1270
Mouse IFN-gamma DuoSet ELISA	R&D Systems	Cat# DY485
Mouse IFN-gamma Quantikine ELISA	R&D Systems	Cat# MIF00
Human IL-12 p70 DuoSet ELISA	R&D Systems	Cat# DY1270
Human IFN-gamma DuoSet ELISA	R&D Systems	Cat# DY285B
Lenti-X p24 Rapid Titer Kit	Takara Bio	Cat# 632200
RNeasy Mini Kit	QIAGEN	Cat# 74104
Deposited data		
Bulk RNA-Seq	Gene expression omnibus (GEO) database	GSE166763
Single cell RNA-Seq	Gene expression omnibus (GEO) database	GSE168297
Experimental models: Cell lines		
M3-9-M	Crystal Mackall, Meadors et al., 2011	N/A
M3-9-M ffluc-eGFP	Murgai et al., 2017	N/A
M3-9-M ffluc-mCherry	This paper	N/A
M3-9-M ffluc-mCherry-OVA	This paper	N/A
KPC177669	NIH Center for Advanced Preclinical Research (CAPR)	N/A
Lenti-X	ATCC	ATCC Cat# CRL-11270, RRID:CVCL_4401
SC	ATCC	ATCC Cat# CRL-9855 RRID:CVCL_6444
Experimental models: Organisms/strains		
Mouse: NCI C57BL/6NCr	Charles River Frederick Research Model Facility	Strain code: 556
Mouse: NCI C57BL/6-cBrd/cBrd/Cr (C57BL/6 albino)	Charles River Frederick Research Model Facility	Strain code: 562
Mouse: B6.SJL-Ptprca Pepcb/BoyJ (Pepboy)	Jackson Laboratory	Stock# 002014
Mouse: C57BL/6-Tg (TcraTcrb)1100Mjb/J (OT-I)	Jackson Laboratory	Stock# 003831
Mouse: B6.Cg-Tg (TcraTcrb)425Cbn/J (OT-II)	Jackson Laboratory	Stock# 004194
Mouse: Rag ^{-/-} OT-I	Taconic Biosciences	Model# 4175
Recombinant DNA		
pRSV-Rev	Dull et al., 1998	RRID:Addgene_12253
pMDLg/pRRE	Dull et al., 1998	RRID:Addgene_12251
pMD2.G	Didier Trono	RRID:Addgene_12259
pFUGW-Pol2-ffLuc2-eGFP	Murgai et al., 2017	N/A
pFUGW-Pol2-ffLuc2-mCherry	Murgai et al., 2017	N/A
pMSCV-OVA	Terry Fry, NCI	N/A
pELNS-Thy1.1	This paper	N/A
pELNS-mIL12-P2A-Thy1.1	This paper	N/A
pELNS-Thy1.1-P2A-mIL12	This paper	N/A

(Continued on next page)

Continued

REAGENT or RESOURCE	SOURCE	IDENTIFIER
Software and algorithms		
FlowJo v10.5 or greater	Tree Star	RRID:SCR_008520; https://www.flowjo.com
Prism version 7.03 or greater	GraphPad	RRID:SCR_002798; https://www.graphpad.com/scientific-software/prism/
Living Image Software	Perkin Elmer	RRID:SCR_014247; https://www.perkinelmer.com/lab-products-and-services/resources/in-vivo-imaging-software-downloads.html
Ingenuity Pathway Analysis	QIAGEN	RRID:SCR_008653; https://digitalinsights.qiagen.com/products-overview/discovery-insights-portfolio/content-exploration-and-databases/qiagen-ipa/
Cell Ranger v3.0.2	10x Genomics	RRID:SCR_017344; https://support.10xgenomics.com/single-cell-gene-expression/software/downloads/latest
Seurat v3.0.2 or greater	Stuart, Butler et al., 2018; Butler et al., 2018	RRID:SCR_007322; http://satijalab.org/seurat/articles/install.html
RStudio	RStudio	RRID:SCR_000432; https://rstudio.com/products/rstudio/download/
R v3.6.0 or greater	The R Foundation	RRID:SCR_001905; https://www.r-project.org
Other		
GentleMACS Dissociator	Miltenyi Biotech	Cat# 130-093-235
LIVE/DEAD Fizable Aqua Dead Cell Stain Kit	Invitrogen	Cat# L34966
Brilliant Violet Stain Buffer	BD Biosciences	Cat# 566385
T Cell TransAct, human	Miltenyi Biotec	Cat# 130-111-160

RESOURCE AVAILABILITY**Lead contact**

Further information and requests for resources and reagents should be directed to and will be fulfilled by the Lead Contact, Rosandra Kaplan (rosie.kaplan@nih.gov).

Materials availability

Reagents generated in this study are available upon request.

Data and code availability

Data generated in this study are available in the Gene Expression Omnibus (GEO) database under the accession numbers GSE166763 for bulk RNA-seq and GSE168297 for scRNA-seq data. All the Software packages and methods used in this study are referenced under Method Details.

EXPERIMENTAL MODEL AND SUBJECT DETAILS**Mice**

6-10-week-old C57BL/6 and C57BL/6 Albino mice were purchased from Charles River at NCI Frederick. B6.SJL-Ptprca Pepcb/BoyJ (Pepboy), C57BL/6-Tg (TcraTcrb)1100Mjb/J (OT-I), and B6.Cg-Tg (TcraTcrb)425Cbn/J (OT-II) mice were purchased from the Jackson Laboratory. RAG^{-/-} OT-I mice were donated by Terry Fry. Male mice were used for all M3-9-M experiments and female mice were used for KPC177669 experiments. All animal experiments were approved by the NCI Animal Care and Use Committee and were conducted in specific pathogen-free conditions at the NIH Animal facility.

Cell lines

M3-9-M embryonal rhabdomyosarcoma cells were derived by Crystal Mackall's group from a tumor in a male transgenic mouse overexpressing hepatocyte growth factor and heterozygous for mutated p53 in the Pediatric Oncology Branch at the National Cancer Institute (NCI) ([Meadors et al., 2011](#)). KPC177669 pancreatic adenocarcinoma cells were derived from a tumor-bearing female KPC mouse ([Lee et al., 2016](#)) by the NCI Center for Advanced Preclinical Research (CAPR). Lenti-X cells were provided by Terry Fry. All cell lines were verified via microarray analysis and routinely tested for mycoplasma. Tumor lines were transduced with pFUGW-Pol2-ffLuc2-eGFP or pFUGW-Pol2-ffLuc2-mCherry and sterile-sorted by fluorescence activated cell sorting (FACS) to establish labeled

cell lines. M3-9-M ffluc-mCherry cells were transduced with a retrovirus encoding ovalbumin (pMSCV-OVA) provided by Terry Fry, stained with PE anti-mouse H-2K^b bound to SIINFEKL (BioLegend), and sorted by FACS to establish the M3-9-M ffluc-mCherry-OVA cell line. All tumor cell lines were cultured in complete RPMI: 10% FBS (Atlantic Biologicals), 1% glutamax (GIBCO), 1% penicillin-streptomycin (GIBCO), 1% non-essential amino acids (GIBCO), 1% sodium pyruvate (GIBCO), 1 mM HEPES (GIBCO), and 50 μM 2-mercaptoethanol (Sigma) at 37°C 5% CO₂. SC (CRL-9855) human peripheral blood monocyte cells were purchased from ATCC. Cells were cultured in IMDM (GIBCO) supplemented with 10% FBS (Atlantic Biologicals), 1% penicillin-streptomycin (GIBCO), HT supplement (GIBCO), and 50 μM 2-mercaptoethanol (GIBCO).

METHOD DETAILS

Tumor models

For M3-9-M orthotopic tumor experiments, mice were injected in the gastrocnemius muscle with 5x10⁵ M3-9-M cells in 100 μL of HBSS (GIBCO). Primary tumors were measured two to three times a week and mice were monitored for survival over time. Tumor volume was calculated as $\frac{4}{3}\pi(X - X_{baseline})(Y - Y_{baseline})(Z)$, where X, Y, and Z are the radius of each dimension of the mouse leg. For lung colonization experiments, 5x10⁴ M3-9-M ffluc-mCherry cells were injected intravenously (i.v.) via tail vein in 200 μL HBSS. For amputation experiments, primary tumors were surgically resected when tumor diameter was approximately 2 cm in the longest direction. For KPC177669 tumor experiments, mice were injected intrasplenically (Soares et al., 2014, Morikawa et al., 1988). Briefly, mice were anesthetized with isoflurane and an 8–10 mm left subcostal incision was made. The spleen was exteriorized and 5x10⁵ KPC177669-ffluc2-mCherry cells were injected in 100 μL HBSS, followed by an additional 100 μL of HBSS to flush the cells into the portal circulation. After two minutes, splenectomy was performed, and the incision was closed in two layers.

Bioluminescent tumor cell tracking

For metastasis experiments, lesions were detected by whole body *in vivo* and postmortem *ex vivo* organ bioluminescence imaging by *in vivo* imaging system (IVIS). Anesthetized mice received a 100 μL intraperitoneal (i.p.) injection of 30 μg/mL D-luciferin (Gold Biotechnology) and were incubated for five minutes. For *ex vivo* tissue imaging, tissues were perfused with PBS, harvested, and incubated in 1 μg/ml D-luciferin in PBS for five minutes. Luminescence was detected by IVIS Lumina Series III (Perkin Elmer) for an exposure time of one minute. Display and image analysis were performed using Living Image Software (Perkin Elmer).

Lentivirus production

We generated genetic constructs encoding the murine or human p40 and p35 IL-12 subunits fused by a linker sequence (Zhang et al., 2015) in the pELNS lentiviral transfer vector under the constitutive EF1α promoter. The murine vector containing murine IL-12 and Thy1.1 reporter protein was synthesized by Genewiz and cloned into the pELNS lentiviral transfer vector. The human lentiviral transfer vector expressing a truncated epidermal growth factor receptor (tEGFR) reporter and human IL-12 was synthesized by GenScript. A construct expressing only Thy1.1 served as a vector control. Lenti-X cells were cultured in high-glucose DMEM supplemented with 10% FBS, 25mM HEPES, 2mM L-glutamine, and 1% penicillin-streptomycin (GIBCO) at 37°C 5% CO₂. The day preceding lentivirus production, 1.8–2x10⁷ cells were seeded onto 150 mm poly-D-Lysine coated plates (Corning). Cells were transiently transfected with Opti-MEM media (GIBCO) containing Lipofectamine 3000 and P3000 (Thermo Fisher Scientific), lentiviral packaging plasmids (pRSV-Rev, pMDLg/pRRE, pMD2.G) and lentiviral vector (Dull et al., 1998). Virus-containing supernatants were harvested at 24 hours and 48 hours, centrifuged to remove cellular debris, and stored at –80°C. For human cell studies, lentivirus was titered by p24 ELISA (Lonza) to determine lentiviral particles (LP) per mL of viral supernatant.

Murine IL12-GEMy production

Bone marrow was flushed from the femurs and tibia of syngeneic mice with collection media (Mg²⁺ Ca²⁺ HBSS with 2% FBS and 1mM EDTA) and enriched for hematopoietic stem and progenitor cells using the magnetic bead-based EasySep Mouse Hematopoietic Progenitor Cell Isolation Kit (StemCell Technologies) per the manufacturer's recommended protocol. The isolated cells were cultured in StemSpan SFEM (StemCell Technologies) media supplemented with 50 ng/mL of mouse SCF, IL-6, and FLT3-L (Bio-Techne) and 1% penicillin-streptomycin. Cells were immediately transduced with lentivirus in the presence of 10 μg/mL protamine sulfate (Fresenius Kabi) and cultured at 37°C for four days. Transduction was confirmed by ELISA for IL-12 p70 (R&D Systems) and by flow cytometry analysis for Thy1.1. In cell tracking experiments, B6.SJL-Ptprca Pepcb/BoyJ (Pepboy) mice were used as donors to track the CD45.1 congenic marker.

Tissue processing

Lungs were perfused with PBS and inflated with digestion medium (HBSS supplemented with 1 mg/mL collagenase I, 20 μg/mL DNase I and Dispase II). Single-cell suspensions were prepared by finely mincing tissues with a scalpel and incubating the tissue on a shaker at 37°C for 20 minutes in 1 mL of digestion media. Tissue was passed through a 70 μM mesh strainer and washed with collection media twice. Tumors were disassociated using a modified protocol as described (Beury et al., 2016). A fragment of the tumor was placed into a gentleMACS C tube (Miltenyi Biotech) containing 5 mL of digestion media. Tumors were then minced with scissors, processed on the gentleMACS dissociator (Miltenyi Biotech) using the program m_impTumor_02. Tubes were secured

in an inverted position and agitated in a 37°C shaker at 100 rpm for 40 minutes. Samples were processed again on the gentleMACS dissociator using program m_impTumor_03, passed through 70 µM cell strainer, and washed with collection media. For spleen, liver, and lymph nodes, tissues were mashed through a 70 µM cell strainer and washed with collection media. For spleen, liver and tumor tissues, red blood cells were lysed with ACK lysis buffer (Life Technologies) for 5 minutes and washed with collection media.

Flow cytometry

Cells were washed with PBS and stained with either Fixable Viability Dye e506 (eBiosciences) or Live/Dead Aqua (Thermo Fisher Scientific) for 30 minutes at 4°C in the dark. Cells were washed in FACS buffer (PBS supplemented with 1% BSA and 0.05% NaN₃), Fc blocking was performed with purified CD16/CD32 antibody (Invitrogen) and a combination of antibodies diluted in either FACS buffer or Brilliant Violet Stain Buffer (BD Biosciences) for 30 minutes at 4°C in the dark. Cells were washed in FACS buffer and analyzed by flow cytometry. If cells were not able to be analyzed on the same day, they were fixed in 4% PFA and analyzed by flow cytometry within three days. Flow cytometry was performed on a BD LSR Fortessa or BD LSRII with the BD High Throughput Sampler (HTS) 96-well plate attachment, when applicable, and analyzed with FlowJo software version 10.5 or greater (Tree Star). In all flow cytometry assays, manual gating was based on fluorescence minus one (FMO) controls.

Cytokine Analysis

Mice were injection with 5x10⁵ unlabeled M3-9-M tumor cells. Vector control and IL12-GEMys were generated from GFP⁺Luciferase⁺ donor mice and 8x10⁶ cells were injected into tumor-bearing mice i.v. on day 12 post primary tumor inoculation. Blood was collected by cardiac puncture, allowed to clot at room temperature, and centrifuged at 2,000 rpm for serum isolation. Lung, spleen, liver, and tumor tissue were harvested and flash frozen at indicated time points. Tissues were weighed then mechanically homogenized in T-PER tissue protein extraction reagent (Thermo Scientific) with HALT protease inhibitor cocktail (Thermo Scientific), centrifuged to pellet cellular debris, and tissue extracts were analyzed by ELISA (R&D Systems).

Chemotherapy treatment

Cyclophosphamide monohydrate (Sigma Aldrich) was prepared to a final concentration of 20 mg/mL in PBS and passed through a 22 µm filter. Fludarabine phosphate (Actavis Pharma, Inc. or Leucadia Pharmaceuticals) was reconstituted with sterile PBS to a final concentration of 50 mg/mL. 100 µL of each was injected per mouse i.p. 2 days prior to IL12-GEMy transfer.

Antibody treatment

For cell depletion studies, mice were injected with 100 µL antibodies i.p. An initial depletion with 200 µg of anti-CD8α antibody clone 2.43, anti-CD4 antibody clone GK1.5, or rat IgG2b isotype control clone LTF-2, or 100 µg of anti-NK1.1 (PK136) (BioXCell) was administered on days 9, 11, and 12 post tumor inoculation. Antibody depletion treatment continued with the administration of 200 µg of antibody every 3-5 days for the duration of the experiment. For IL-12 blocking studies, 1 mg per mouse of InVivoMAb anti-mouse IL-12 p75 (R2-9A5) or InVivoMAb rat IgG2b isotype (LTF-2) (BioXCell) was administered i.p. on day 12 post tumor inoculation and every 5 days for the duration of the experiment.

T cell co-culture experiments

Naive splenocytes from OT-I or OT-II mice were co-cultured with non-transduced control myeloid cells or IL12-GEMys at various ratios in the presence of 1 µg/mL OVA₂₅₇₋₂₆₄ (SIINFEKL) or OVA₃₂₃₋₃₃₉ peptide, respectively (AnaSpec, Inc), in complete RPMI (GIBCO). To generate activated T cells, splenocytes were first cultured in the presence of 1 µg/mL peptide (AnaSpec, Inc) and 50 units/mL of recombinant IL-2 (Clinigen) for 4 days prior to co-culture with myeloid cells in the presence of 1 ng/mL cognate peptide. Supernatant from co-cultures was collected after 24 hours and IFNγ was quantified by ELISA (R&D Systems).

T cell activation for adoptive transfer

Spleens from Rag^{-/-} OT-I mice were harvested and processed into single cell suspension as described above. Splenocytes were activated in complete RPMI in the presence of 50 units/mL recombinant IL-2 (Clinigen) and 1 µg/mL OT-I cognate peptide OVA₂₅₇₋₂₆₄ (SIINFEKL) or OT-II cognate peptide OVA₃₂₃₋₃₃₉ for four days (AnaSpec, Inc). Activated OT-I T cells were transferred into mice i.v. via tail vein.

Immunofluorescence

Lungs were harvested and fixed in 10% formalin for 24 hours. Fixed lungs were embedded in paraffin and 8-µM thick sections were prepared for staining (VitroVivo Biotech). Slides were stained using the Opal 7-Color Manual IHC Kit (PerkinElmer) per the manufacturer's instructions. Briefly, slides were deparaffinized and rehydrated in a series of xylene and ethanol gradients, microwaved in Rodent Decloaker (Biocare Medical) and then cooled. Slides were washed with water and then TBST (TBS + 0.05% Tween-20) followed by blocking with Bloxall Blocking Solution (Vector Laboratories). Staining with primary and secondary antibodies and OPAL fluorophores were performed per the manufacturer's instructions. The following antibodies were used: CD4 (Invitrogen, clone 4SM95; 1:100), CD8 (Invitrogen, clone 4SM16; 1:100), ImmPRESS HRP Goat anti-rat IgG (Vector Laboratories; 1:4). All images were collected on a Zeiss 880/Airyscan Microscope at the CCR Microscopy Core Facility using the 20X and 40X objectives. For quantitation, the 20X

images were used to manually count the number of CD4 and CD8 cells and calculate nuclear area using color thresholding in ImageJ (NIH).

Bulk RNA sequencing

Naive or tumor-bearing mice were treated or not with 8×10^6 IL12-GEMys on day twelve post tumor inoculation ($n = 4$ mice per group). Mice were euthanized three days after IL12-GEMy transfer and lungs were harvested. For bulk RNA sequencing (RNA-seq), lungs were flash-frozen in liquid nitrogen. Tissue was homogenized in TRIzol (Thermo Fisher) and RNA was isolated by chloroform extraction followed by the RNeasy Mini Kit (QIAGEN) according to manufacturer's recommendations. 3' library preparation was performed using the Illumina TruSeq Stranded mRNA kit and Hiseq4000 platform (Illumina) at a total of 100 million reads per sample according to standard operating procedure at the CCR Genomics core facility. Alignment, normalization, and primary gene expression analysis were performed as previously described (Murgai et al., 2017) utilizing the computational resources of the NIH HPC Biowulf cluster (<https://hpc.nih.gov/>). Pathway analysis was performed using Ingenuity Pathway Analysis (QIAGEN) on gene sets with a greater-than-two-fold change and p value cut off of 0.05.

Gene set enrichment analysis

In each RNA-seq profile from the lungs of treated and non-treated tumor-bearing mice, we ranked genes in descending order based on their log-fold change in expression compared to non-tumor-bearing control mice. We tested the enrichment of selected pathways using the fgsea package (Korotkevich et al., 2019) in R, where 10,000 permutations were used to compute enrichment p values for each pathway. Pathways with an adjust enrichment p value less than 0.1 were considered to be significantly enriched.

Pre-metastatic niche gene signature

We derived two 50-gene pre-metastatic niche gene sets, referred to as Up-regulated and Down-regulated gene sets, by picking 50 genes that showed the highest log-fold changes in expression between lungs of non-treated tumor-bearing and control mice. To validate these gene sets, we analyzed a collection of published bulk RNA-seq and microarray-based gene expression profiles from pre-metastatic niches. Normalized microarray and bulk RNA-seq expression profiles for each dataset were downloaded using the GEOquery package in Bioconductor (Davis and Meltzer, 2007, Gentleman et al., 2004). We log-transformed expression values from raw FPKM values to units of $\log(1 + \text{FPKM})$ in RNA-seq datasets and used the author-submitted normalized expression values in microarray-based datasets. In datasets that contained replicates, we computed the average expression, after which we computed log-fold changes of gene expression between pre-metastatic and control samples. We then used a one-sided Wilcoxon test to check if genes in the Up-regulated (or Down-regulated) gene set had a higher (or lower) log-fold change than genes in the rest of the genome.

Single-cell RNA sequencing

Lungs from naive or tumor-bearing mice with or without IL12-GEMy treatment ($n = 4$ mice per group) were processed into single-cell suspension and oligodT-based cDNA libraries were barcoded by droplet-partitioning using the Chromium Single Cell Controller (10x Genomics) system at the NCI-CCR Single Cell Analysis Facility. Dead cell removal was performed, and samples were incubated with TotalSeq-A hashtag oligos (HTOs) (BioLegend). Two biological replicates were run together per capture lane. Sequencing was performed on the NovaSeq (Illumina) at the NCI-CCR Sequencing Facility. Sequencing read demultiplexing, alignment to mm10 (Ensembl Ref annotation 93), and generation of a unique-molecular-index-collapsed gene expression matrix was performed using Cell Ranger version 3.0.2 (10x Genomics). Additional data processing and analysis was performed using Seurat v3.0.2 (Butler et al., 2018, Stuart et al., 2019) in RStudio running R v3.6.0. In short, each sample set was filtered for cell barcodes with greater than 500 genes detected and less than 20% percent mitochondrial gene expression. Cell barcodes with either no cell hashing antibody detected or multiple were excluded from the analysis. Data from all samples were merged, and normalization and scaling was performed using SCTransform (Christoph Hafemeister, 2019). Clustering and UMAP projections were performed on combined data, with collapsing of biologically relevant clusters informed by clustree empirical analysis. Cell type / cluster marker gene detection was performed with FindAllMarkers () in Seurat with Wilcoxon ranked sum test. Differential expression testing across conditions for each cluster performed with MAST (Finak et al., 2015). Single cell plots generated within Seurat using ggplot2 (Hadley, 2016). Analysis notebooks available on request.

Comparison of IL12-GEMy bulk data with scRNA-seq data

We created a comparison gene set to compare the IL12-GEMy product with cells in our scRNA-seq data. We first picked a set of the 3,000 most variable genes, determined by the SCTransform (Christoph Hafemeister, 2019) function in Seurat, across all 70,370 cells in our scRNA-seq data. Out of these 3,000 genes, 1,884 were annotated and expressed in the bulk sequencing of the IL12-GEMy product, which formed our comparison gene set. To overcome noise from transcript drop-outs in the scRNA-seq data, we utilized a bootstrapping approach where we picked 90% of cells in each cluster and averaged the SCTransformed expression values of each gene in the comparison gene set. We repeated this process 100 times to generate 100 groups of cells for each cluster. We computed the cosine similarity between the average gene expression of each bootstrapped group with the IL12-GEMy bulk RNA-seq profile. Since the gene expression values are all non-zero, the cosine similarity ranges between 0 and 1, with a higher score indicating greater

similarity between gene expression profiles. We then averaged the cosine similarity scores across all bootstrap groups to obtain a single similarity score between the IL12-GEMy product and each scRNA-seq cluster.

Human IL12-GEMy product

SC (CRL-9855) human peripheral blood monocyte cells were transduced with vector control or tEGFR-IL12 lentivirus for 24 hours at varying multiplicities of infection (MOI). MOI was calculated from p24 titer as lentiviral particles (LP) per cell. Transduction efficiency was measured by flow cytometry staining of human cetuximab biosimilar EGFR antibody (R&D Systems). IL-12 production was measured in the supernatant by ELISA (R&D Systems).

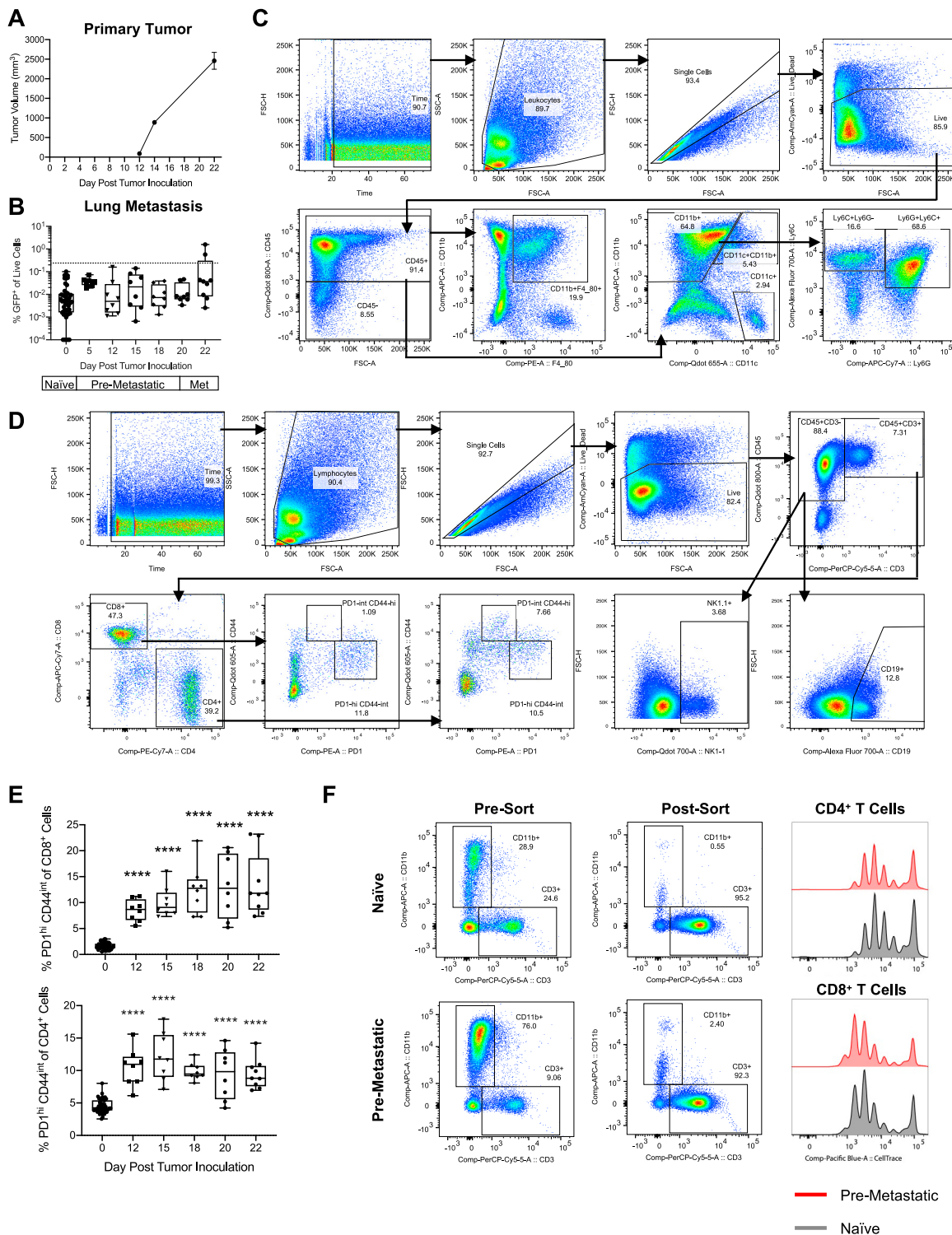
Human IL12-GEMy co-culture with lymphocytes

Primary human elutriated lymphocytes from healthy donors were acquired from the NIH Department of Transfusion Medicine. Vector control or tEGFR-IL12 SC cells were transduced at a MOI of 150 LP/mL for 24 hours. Lymphocytes were incubated overnight in Stem-Span SFEM II media supplemented with gentamicin and 10 units/mL of recombinant human IL-2 (Clinigen). T cells were activated with 12.5 μ L/mL T Cell TransAct beads (Miltenyi Biotec) and 40 units/mL of recombinant human IL-2 and co-cultured at varying GE-My:Lymphocyte ratios. Supernatant was collected at 24 hours and analyzed for IFN- γ production by ELISA (R&D Systems).

Statistical analysis

All statistical analysis was performed in Prism version 7.03 or greater (GraphPad Software). Graphs represent mean values \pm standard error. P values were calculated for bar graphs using Kolmogorov-Smirnov test, unpaired two-tailed Student's t test, one-way ANOVA, or Kruskal-Wallis test, and log-rank statistics for survival analyses, as indicated in figure legends. In boxplots, the center line represents the median, the box limits denote the 25th to the 75th percentile and the whiskers represent the minimum and maximum value. For scRNA-seq data, statistical differences between groups analyzed by Wilcoxon test. $p < 0.05$ was considered statistically significant. * $p \leq 0.05$, ** $p \leq 0.01$, *** $p \leq 0.001$, **** $p \leq 0.0001$.

Supplemental figures

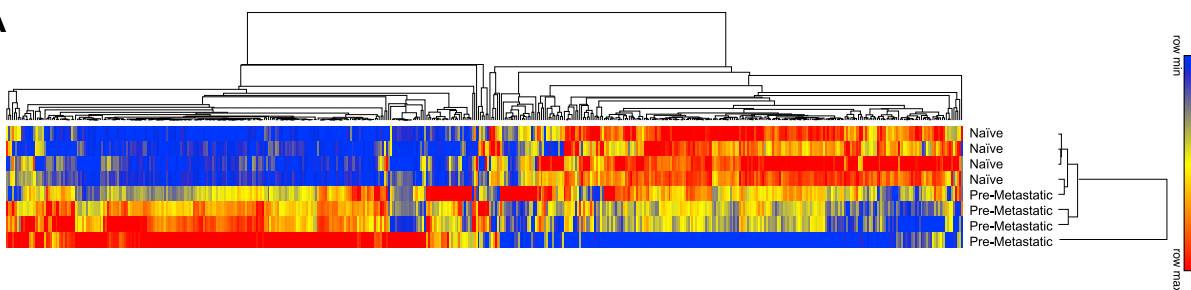


(legend on next page)

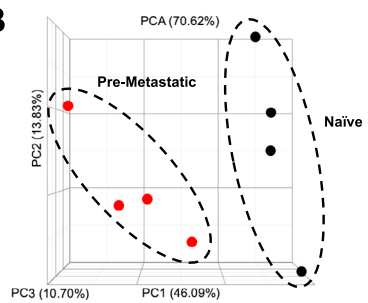
Figure S1. Flow cytometry characterization of immune populations in pre-metastatic lungs, related to Figures 1A and 1B

(A) Tumor volume measurements of mice that were injected with M3-9-M ffluc-eGFP rhabdomyosarcoma primary tumor orthotopically in the gastrocnemius muscle of the leg. (B) M3-9-M ffluc-eGFP tumor cells detected in the lungs of mice by flow cytometry, gated on live, single, CD45⁻ cells. The dashed line represents the threshold of metastatic lesions that were visible to the naked eye. In boxplots, the center line represents the median, the box limits denote the 25th to the 75th percentile, and the whiskers represent the minimum and maximum value. The gating strategy for (C) myeloid and (D) lymphocyte flow cytometry staining panels are shown. Arrows indicate the parent population that the subsequent plot is gated on. Gates were drawn manually based on fluorescence minus one (FMO) controls. (E) The expression of T cell activation markers PD1 and CD44 over time after IL12-GEMy treatment. In boxplots, the center line represents the median, the box limits denote the 25th to the 75th percentile and the whiskers represent the minimum and maximum value. All populations are gated on live CD45⁺CD3⁺ single cells. Data were analyzed by ordinary one-way ANOVA with Dunnett's multiple comparisons test between the mean of day 0 and each time point. (F) T cells were isolated from naive or M3-9-M tumor-bearing mice on day 18 post tumor inoculation by magnetic bead negative selection. Cells were pulsed with CellTrace Violet and activated with Mouse T-Activator CD3/CD28 beads at a 1:1 ratio in the presence of 10 ng/mL of IL-7 for 3 days. Cell proliferation was analyzed by flow cytometry gating on CD4⁺ or CD8⁺ T cells.

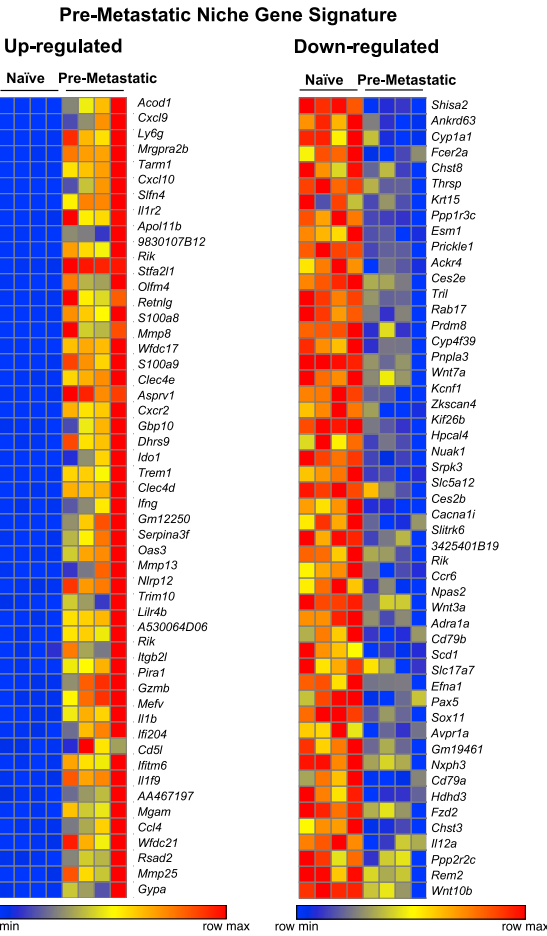
A



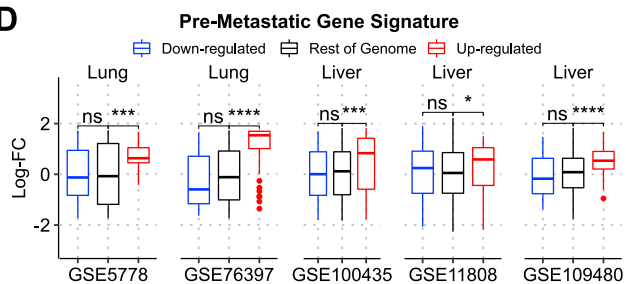
B



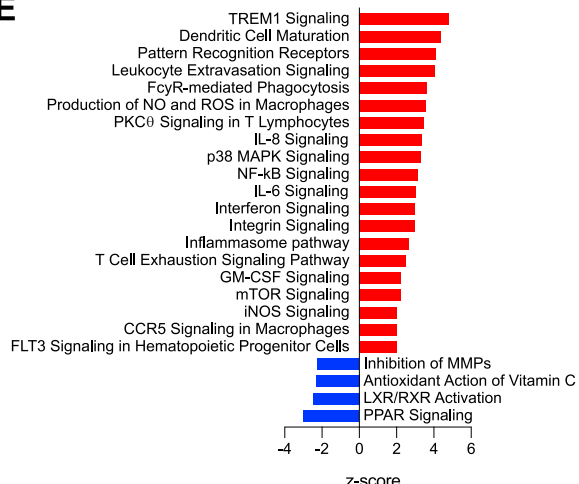
C



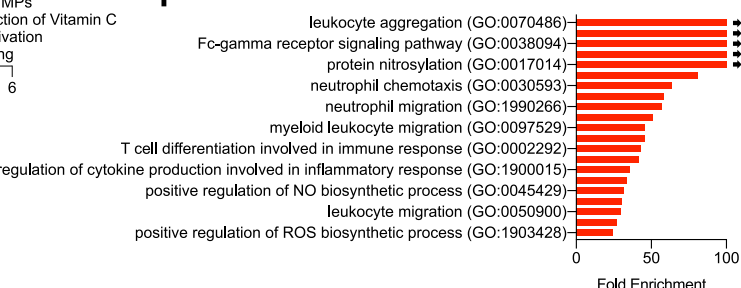
D



E



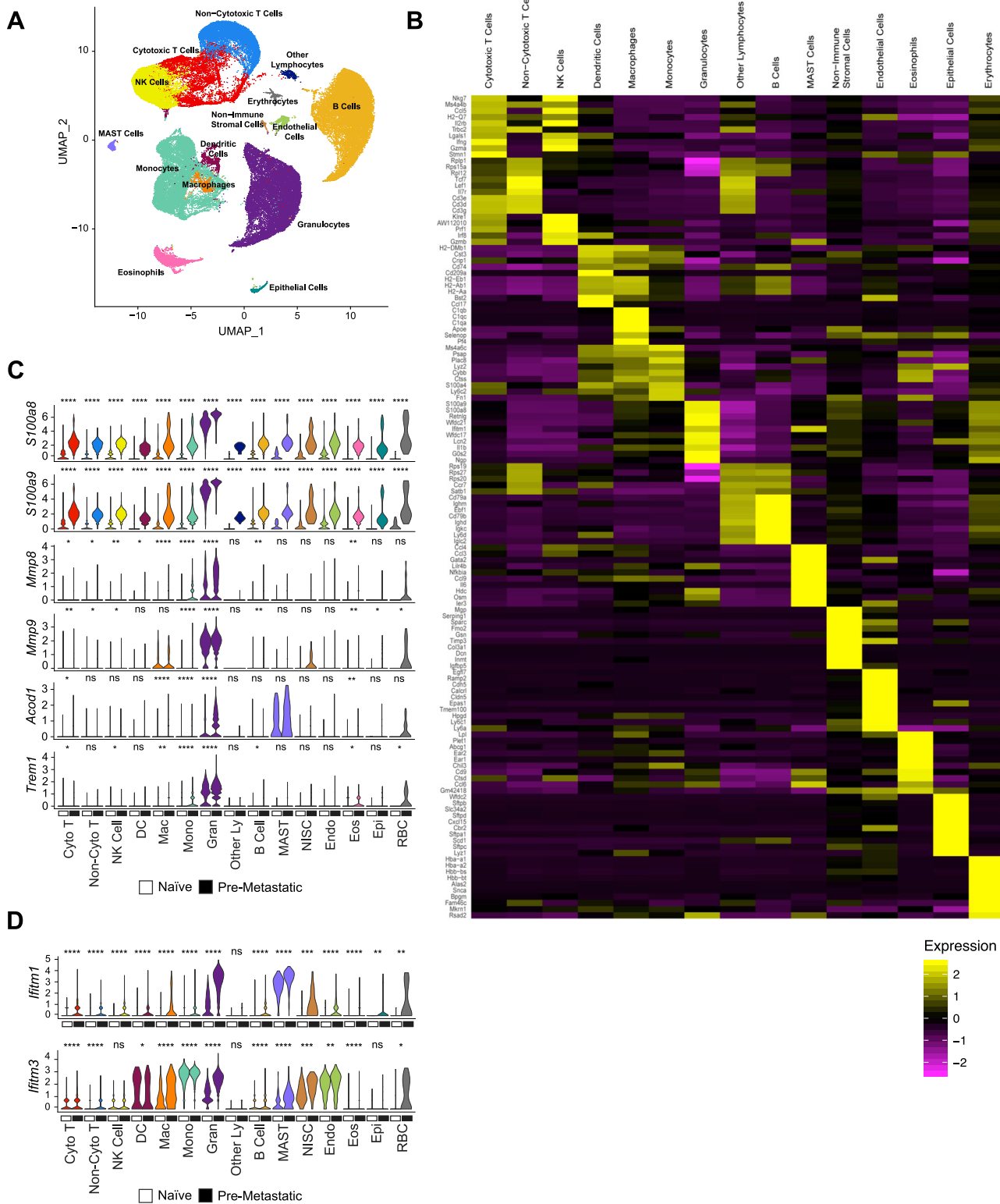
F



(legend on next page)

Figure S2. Transcriptional programs are drastically altered in pre-metastatic lungs, related to Figures 1C and 1D

(A) Hierarchical clustering by one minus Pearson correlation of the top 500 differentially expressed genes from bulk RNA sequencing of lungs from pre-metastatic versus naive mice. (B) Principle component analysis (PCA) was performed using Partek Flow. (C) The top 50 genes with the highest fold change increase and decrease in the lungs of tumor-bearing versus naive mice. Only genes with a p value < 0.05 are shown. (D) Log-fold changes of the top 50 genes upregulated in pre-metastatic lungs (red) and the top 50 genes downregulated in pre-metastatic lungs (blue) in published datasets. P values were determined using a one-sided Wilcoxon rank-sum test. (E) Select pathways from Ingenuity pathway analysis (IPA) of differentially expressed genes between pre-metastatic and naive lungs. Red bars indicate positive z-scores; blue bars indicate negative z-scores. (F) Database for Annotation, Visualization and Integrated Discovery (DAVID) Gene Ontology (GO) analysis of the top 50 genes upregulated in pre-metastatic compared to naive lungs. Relevant, significantly changed GO terms associated with pre-metastatic lungs are shown. Arrows indicate >100-fold enrichment.

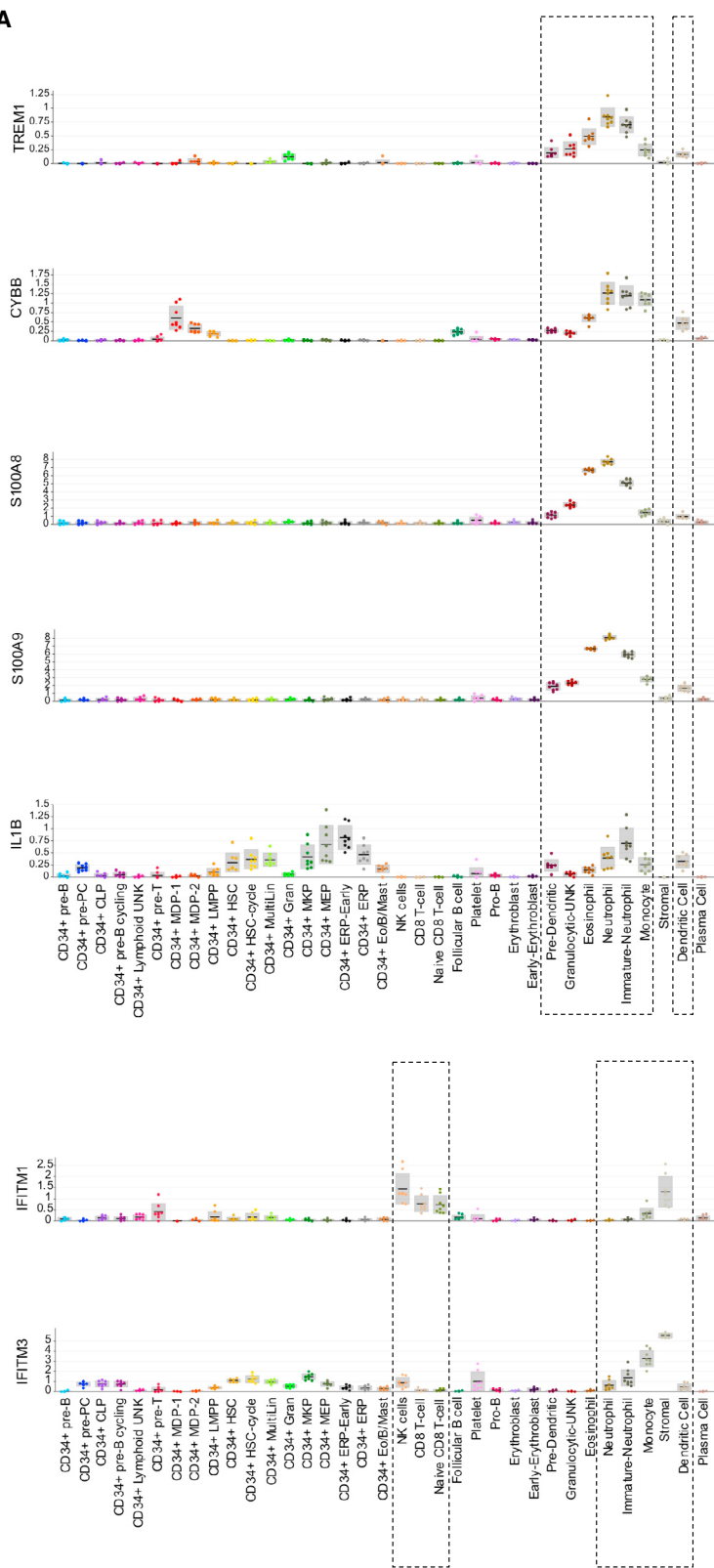


(legend on next page)

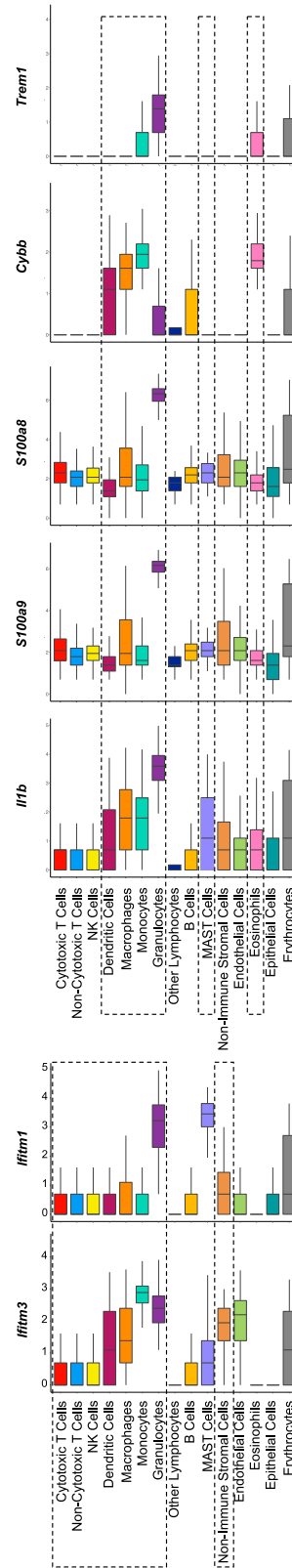
Figure S3. Single-cell RNA sequencing cluster identification and expression of pre-metastatic signature genes associated with immune suppression, related to Figures 1E–1G

(A) UMAP plot of combined samples color-coded to indicate cluster identity annotations. (B) Heatmap displaying the top 10 genes used to define each cluster. (C–D) Violin plots of genes associated with immune suppression. Statistical differences between groups analyzed by Wilcoxon test. **** $p < 0.0001$; *** $0.0001 < p < 0.001$; ** $0.001 < p < 0.01$; * $0.01 < p < 0.05$.

A



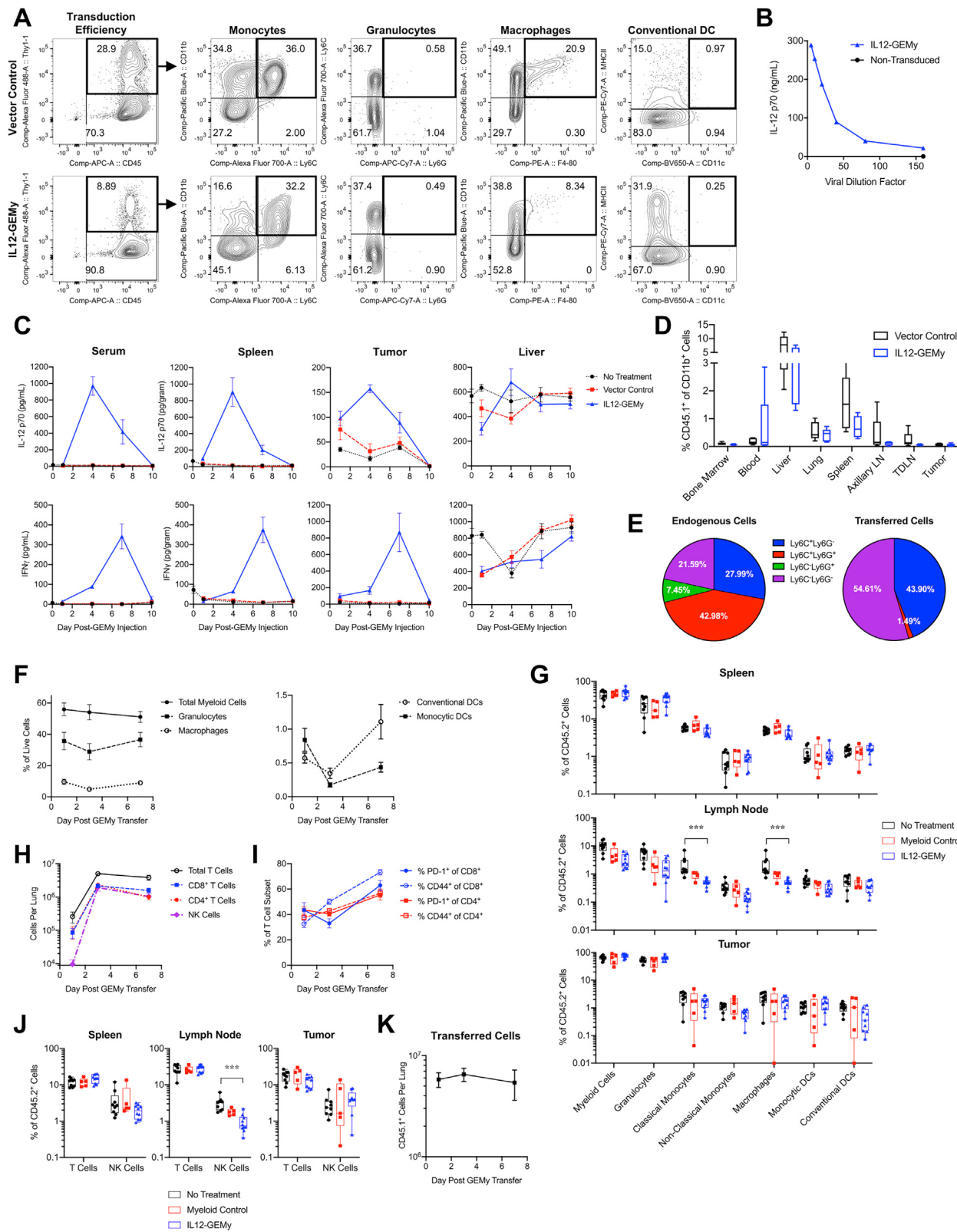
B



(legend on next page)

Figure S4. Immune suppression genes found in the pre-metastatic lung are also present in the hematopoietic stem cell niche of the bone marrow in humans, related to Figure 1

(A) Data from normal human bone marrow was queried using the Human Cell Atlas bone marrow single-cell interactive web portal⁸⁰ (B) Gene expression data of select transcripts per cluster in pre-metastatic lungs. In boxplots, the center line represents the median, the box limits denote the 25th to the 75th percentile, and the whiskers represent the minimum and maximum value.



(legend on next page)

Figure S5. IL12-GEMy phenotype, cytokine production, and impact on immune cell populations *in vivo*, related to Figure 2

(A) Cells transduced with Thy1.1 vector control or Thy1.1-IL12 were harvested after 4 days in culture and analyzed by flow cytometry. Representative images are shown. Transduction efficiency was consistent between experiments. (B) Cells were transduced with various dilutions of IL-12-encoding lentivirus for 4 days and assessed for IL-12 secretion by ELISA. (C-D) 8×10^6 IL12-GEMy or vector control cells were adoptively transferred into mice on day 12 post tumor inoculation. (E) Tissues were harvested, flash frozen, homogenized in tissue protein extraction reagent with HALT protease inhibitor (Thermo Fisher Scientific), and evaluated by ELISA (R&D Systems). (D) CD45.1⁺ transferred cells as a percentage of live cells 24 h after transfer of 8×10^6 cells. (E) The phenotype of endogenous myeloid cells and transferred IL12-GEMys in the lungs of tumor-bearing mice by flow cytometry 24 h after transfer of 8×10^6 cells. (F) 1.85×10^6 IL12-GEMys were transferred into M3-9-M ffluc-mCherry tumor-bearing mice on day 11 post tumor inoculation. Lungs were harvested one, three, and seven days post-treatment. Myeloid populations analyzed by flow cytometry gated on live CD45⁺ single cells (Myeloid = CD11b⁺CD11c⁻, Granulocytes = CD11b⁺Ly6G⁺, Monocytic Dendritic Cells = CD11b⁺CD11c⁺, Conventional Dendritic Cells = CD11b⁻CD11c⁺, Macrophages = CD11b⁺CD43⁺Ly6C⁺F4/80⁺). (G) Mice were inoculated with M3-9-M ffluc-mCherry tumor and not treated ($n = 9$) or treated with non-transduced myeloid cells ($n = 5$) or IL12-GEMys ($n = 10$) on days 12, 19, and 26 (4.1×10^6 , 2.8×10^5 , and 5×10^6 IL12-GEMy cells at each time point, respectively). Tissues were harvested on day 27 and analyzed by flow cytometry gated on live CD45⁺ single cells. Myeloid cell populations in the spleen, non-draining inguinal lymph node, and tumor (Myeloid = CD11b⁺CD11c⁻, Granulocytes = CD11b⁺Ly6G⁺, Monocytic Dendritic Cells = CD11b⁺CD11c⁺, Conventional Dendritic Cells = CD11b⁻CD11c⁺, Non-Classical Monocytes = CD11b⁺CD43⁺Ly6C⁻, Classical Monocytes = CD11b⁺CD43⁺Ly6C⁺, Macrophages = CD11b⁺CD43⁺Ly6C⁺F4/80⁺). Data were analyzed by multiple Kolmogorov-Smirnov tests. (H) Experiment as described in F. Lymphoid populations (T Cells = CD3⁺, CD8⁺ T cells = CD3⁺CD8⁺, CD4⁺ T Cells = CD3⁺CD4⁺, NK Cells = CD3⁻NK1.1⁺) and (I) lymphocyte activation markers PD-1 and CD44 in the lung are shown. (J) Experiment as described in G. T and NK cells in the spleen, non-draining inguinal lymph node and tumor (T Cells = CD3⁺, NK Cells = CD3⁻NK1.1⁺). Flow cytometry data were analyzed by multiple Kolmogorov-Smirnov tests. (K) Experiment as described in F. CD45.1⁺ transferred cells were analyzed by flow cytometry. *** $p < 0.0001$; ** $0.0001 < p < 0.001$; ** $0.001 < p < 0.01$; * $0.01 < p < 0.05$. In line graphs, data are represented as mean \pm SEM. In boxplots, the center line represents the median, the box limits denote the 25th to the 75th percentile and the whiskers represent the minimum and maximum value.

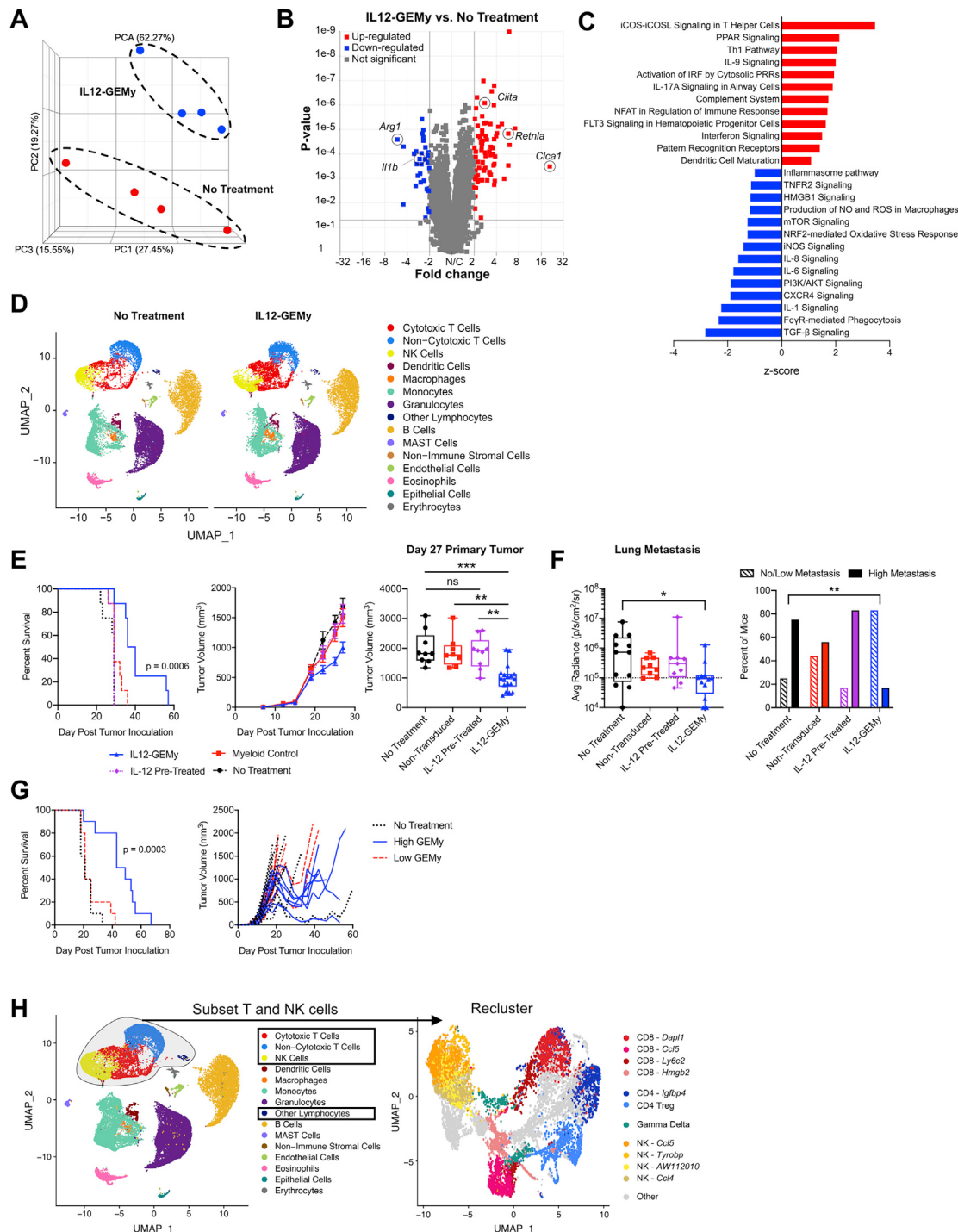


Figure S6. Transcriptional changes in pre-metastatic lungs in response to IL12-GEMy treatment, IL-12 pre-treatment, and dosing experiments, related to Figures 3A, 3C, and 4

(A-C) RNA was isolated and sequenced from the lungs of mice that were naive, tumor-bearing, or tumor-bearing treated with 8×10^6 IL12-GEMys. (A) Principle component analysis (PCA) was performed using Partek Flow on non-treated and IL12-GEMy-treated mice. (B) Volcano plot of differential gene expression between IL12-GEMy treated and non-treated mice. (C) Select pathways that are significantly up and downregulated in IL12-GEMy-treated mice by Ingenuity pathway analysis (IPA). (D) ScRNA-seq was performed on lungs from tumor-bearing mice or tumor-bearing mice treated with 8×10^6 IL12-GEMys 3 days post IL12-GEMy treatment, 15 days post tumor inoculation. UMAP plots of single cell RNA sequencing analysis of lungs from non-treated and IL12-GEMy-treated mice. (E-F) Mice were orthotopically inoculated with 5×10^5 M3-9-M ffluc-mCherry cells and treated with equal numbers of control myeloid cells, myeloid cells cultured in the presence of 10 ng/mL IL-12, or IL12-GEMys on days 12, 19, and 26 post tumor inoculation (4.1×10^6 , 2.8×10^5 , and 5×10^6 cells at each time point,

(legend continued on next page)

respectively). (E) Mice were followed for primary tumor growth and survival ($n = 8$). Primary tumor volume was analyzed on day 27 by Kruskal-Wallis test with Dunn's multiple comparisons test (no treatment: $n = 12$, myeloid: $n = 9$, IL-12 pre-treated: $n = 9$, IL12-GEMy: $n = 12$). (F) Lung metastasis was assessed by bioluminescent imaging *ex vivo* by IVIS on day 27. Pictures of lungs were normalized, visually inspected for bioluminescence, and categorically grouped into high metastasis (presence of bioluminescence) or no/low metastasis (no bioluminescence). Statistical analysis was determined by Fisher's exact test. (G) M3-9-M ffluc-mCherry mice were treated with low dose (1×10^6) or high dose (8×10^6) of IL12-GEMys and followed for survival and tumor growth. Survival was analyzed by Log-rank (Mantel-Cox) test. (H) Experiment as described in D. Cytotoxic T cell, Non-Cytotoxic T cell, NK cell, and Other Lymphocyte clusters were subsetted from the whole lung scRNA-seq analysis and reclustered to identify more specific cell subsets. *** $p < 0.0001$; ** $0.0001 < p < 0.001$; ** $0.001 < p < 0.01$; * $0.01 < p < 0.05$. In line graphs, data are represented as mean \pm SEM. In boxplots, the center line represents the median, the box limits denote the 25th to the 75th percentile and the whiskers represent the minimum and maximum value.

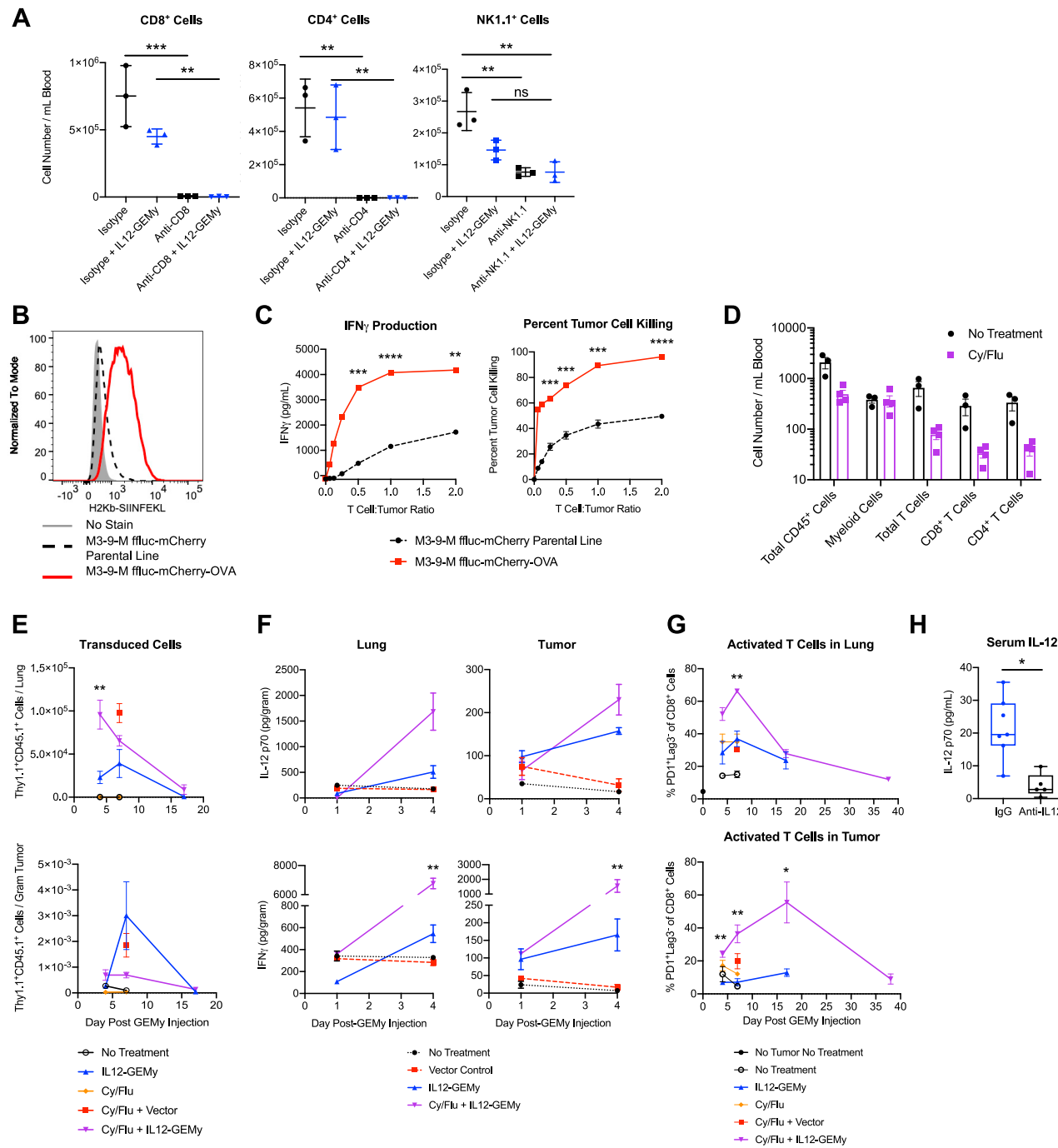


Figure S7. Validation of IL12-GEMy treatment models, related to Figures 6

(A) M3-9-M ffluc-mCherry tumor-bearing mice were treated with three doses of isotype, anti-CD8, anti-CD4 or anti-NK1.1 antibody i.p. on days 9, 11, and 12 post tumor inoculation. 8×10^6 IL12-GEMys were transferred on day 12. Isotype, anti-CD8, and anti-CD4 were also administered on day 15 in accordance with the treatment schedule. Blood was collected one week after the initiation of the depletion therapy and immune cell populations were analyzed by flow cytometry. Statistical analysis was performed by ordinary one-way ANOVA with Tukey's multiple comparisons test. (B) M3-9-M ffluc-mCherry cells were transduced with the lentiviral vector containing ovalbumin (OVA). SIINFEKL-positive cells were sorted by FACS to establish the M3-9-M ffluc-mCherry-OVA cell line. The expression of the ovalbumin peptide SIINFEKL in the context of H2-K^b on the surface of the transduced cells was measured by flow cytometry. (C) Splenocytes from OT-I mice were activated in culture with 1 μ g/mL SIINFEKL peptide and 50 units/mL of recombinant IL-2. M3-9-M ffluc-mCherry and M3-9-M ffluc-mCherry-OVA cells were plated and allowed to adhere overnight. OT-I cells were collected on day 5 post-activation and plated onto the tumor cells at the indicated ratios. Supernatant was collected at 24 h and analyzed by ELISA for IFN γ . After the supernatant was removed, luciferin was added to the cells and luminescence was recorded as a readout for luciferase-expressing tumor cell abundance. Percent tumor killing was calculated as follows: $100 - [(tumor cells + T cells) / (tumor cells alone) \times 100]$.

(legend continued on next page)

Statistics were calculated by unpaired t test at each ratio. (D) Non-tumor-bearing mice were treated with 2 mg of cyclophosphamide and 5 mg of fludarabine i.p., and immune cell populations in the blood were analyzed by flow cytometry 48 h after treatment. There were no significant differences by Kolmogorov-Smirnov test. (E-G) 8×10^6 IL12-GEMy or vector control cells were adoptively transferred into mice on day 12 post M3-9-M ffluc2-mCherry tumor inoculation, 2 days following Cy/Flu administration. (E) Tissues were harvested at 4, 7, and 17 days after IL12-GEMy injection and processed for flow cytometry ($n = 4-8$ mice per group). Cells are gated on live, single cells. Transduced cells were detected by gating on Thy1.1 $^+$ CD45.1 $^+$ cells. Statistical analysis was performed between the IL12-GEMy and Cy/Flu+IL12-GEMy groups by Kolmogorov-Smirnov test at each time point. (F) Tissues were harvested, flash frozen, homogenized, and evaluated by ELISA. Statistical analysis was performed between the IL12-GEMy and Cy/Flu+IL12-GEMy groups by Kolmogorov-Smirnov test ($n = 3-5$ mice per group). (G) Tissues were harvested at 4, 7, 17, and 38 days following IL12-GEMy treatment and processed for flow cytometry staining. Cells are gated on live, single, CD45.2 $^+$, CD3 $^+$, CD8 $^+$, PD1 $^+$, Lag3 $^-$ cells. Statistical analysis was performed between the IL12-GEMy and Cy/Flu+IL12-GEMy groups by Kolmogorov-Smirnov test. (H) Mice were treated with Cy/Flu on day 10 and 8×10^6 IL12-GEMys on day 12 post tumor inoculation. Anti-mouse IL-12 p75 or rat IgG2b isotype was administered i.p. on day 12 post tumor inoculation and every 5 days for the duration of the experiment. Serum was collected on day 104 post-tumor inoculation, day 92 post treatment with 8×10^6 IL12-GEMys, 2 days after antibody treatment, and IL-12 was analyzed by ELISA (R&D Systems). Statistics were calculated using the Kolmogorov-Smirnov test. *** $p < 0.0001$; ** $0.0001 < p < 0.001$; * $0.001 < p < 0.01$; * $0.01 < p < 0.05$. In bar and line graphs, data are represented as mean \pm SEM. In boxplots, the center line represents the median, the box limits denote the 25th to the 75th percentile and the whiskers represent the minimum and maximum value.